TECHNICAL MEMORANDUM

254

Introduction of revised radiation, convection, cloud and vertical diffusion schemes into Cy18r3 of the ECMWF integrated forecasting system

D. Gregory, J-J. Morcrette, C. Jakob and A. Beljaars

Research Department

July 1998

European Centre for Medium-Range Weather Forecasts
Europäisches Zentrum für mittelfristige Wettervorhersage
Centre européen pour les prévisions météorologiques à moyen

Introduction of Revised Radiation, Convection, Cloud and Vertical Diffusion Schemes into Cy18r3 of the ECMWF Integrated Forecasting System

D. Gregory, J.J. Morcrette, C. Jakob and A. Beljaars

May 1998

ABSTRACT

Revisions to the radiation, convection, cloud and vertical diffusion schemes introduced into Cy18r3 of the ECWMF Integrated Forecasting System are briefly described. The impact of the changes upon modelled seasonal climate is considered using T63 simulations of June/July/August 1987 and December/January/February 1987/88. The revised physics leads to substantial changes which are of benefit to both coupled-ocean atmosphere simulations and medium-range forecasts. The distribution of tropical precipitation is improved, as is the tropical flow and structure of the Hadley circulation. Changes to the cloud distribution, together with the revised radiation scheme lead to better agreement between modelled and observed fluxes at the Top of the Atmosphere and at the surface. During December/January/February 1987/88, the westerly flow in the upper troposphere of the eastern Pacific is better captured. The impact of the revised physics package upon T213 10-day forecasts using an experimental version of a 4D-Variational analysis system is also considered. The impact upon medium-range forecast performance is rather neutral, although temperature biases are generally reduced. The intensification of the ITCZ in the Pacific and Atlantic throughout the forecast is reduced when the revised physics package is included. The study demonstrates part of the methodology used in testing new parametrizations for use in the ECMWF model and also the benefit of considering both the impact of parametrizations upon seasonal and medium-range forecasts.

1. INTRODUCTION

In recent years, together with changes to the data assimilation system and to the dynamical component of the model, changes to the parametrizations of the ECMWF model have brought about improved model performance (such as the revised sub-grid scale orography and prognostic cloud schemes introduced in April 1995). This paper describes revisions to the radiation, convection, cloud and vertical diffusion schemes used in the ECMWF Integrated Forecasting System (IFS), which collectively are referred to as "PACKAGE F".

The revisions were undertaken for several reasons. Firstly to improve the physical basis of the parametrizations and their performance as measured against observations and detailed models (such as line-by-line radiation codes and fine-scale cloud resolving models for convection). Secondly the changes were aimed at correcting errors in the Top of Atmosphere (TOA) and surface energy budget, important for coupled ocean-atmosphere simulations of the model used in seasonal forecasting activities at ECMWF. Some aspects of the medium-range forecast performance of the model are also improved.

A brief description of the changes is given. Each of these had undergone a wide range of tests in either single column models or in case studies with the IFS, with evaluation of their performance being measured against data from detailed physical models and/or observations. These studies are not considered in detail here, the focus being the impact of the parametrizations upon the performance of the IFS in seasonal and medium-range forecasts. In this it demonstrates something of the methodology used at ECMWF when testing revised parametrizations in the IFS. Although some indication is given of the impact of individual changes, greater emphasis is placed upon the impact of the combined package. Section 3 describes the impact of the revised physics package on T63 seasonal simulations while in section 4, the

impact of the package upon 10 day T213 forecasts using an experimental version of the 4D-Variational analysis system (incorporated into the operational version of the IFS in early December 1997) is considered.

2. DESCRIPTION OF MODIFIED PHYSICS ("PACKAGE F")

2.1 RADIATION SCHEME

The changes described improve the physical basis of the scheme and correct some known biases associated with the radiation code used in the IFS since April 1989.

2.1.1 Change to the surface longwave emissivity

Currently the longwave (LW) emissivity of the surface in the ECMWF model is set to 0.996, over the whole LW spectrum, irrespective of the conditions of surface type, surface moisture, etc. This value corresponds to the pre-1970's value for water, as for example reported by *Kondratyev* (1972). However, it is known that the LW window emissivity for land surfaces can differ substantially from unity depending on the surface characteristics and soil moisture, and that even ocean water may differ from this high value. Recent work, usually targeted at defining boundary conditions for remote sensing (*Masuda et al.*, 1988; *Rees and James*, 1992; *Rees*, 1993a, 1993b), all report emissivity values which vary with the surface type and which for some surfaces are much lower than the current model value. Consequently the model emissivity has been modified in two respects: (1) to account for different values of the surface LW emissivity according to the surface type, and (2) to account for the variation of spectral emissivity (ε_W) in the longwave window region (800-1250 cm^{-1}) with the soil moisture content. Given the recent observations over ice-free ocean, sea-ice, and snow-covered land, it is proposed to use a value of 0.99 outside the window region and set the window emissivity to 0.98 for ocean, sea ice and snow. The longwave *window* emissivity of the land surface was reconsidered from various references (*Kondratyev*, 1972; *Taylor*, 1979; *van de Griend et al.*, 1989). Over land it is reduced from 0.996 to 0.96. However over desert regions, defined as areas with null vegetation and a surface albedo larger than 30 percent, with null snow cover and a soil moisture content equal to the minimum soil water holding, the value of surface longwave window emissivity is further reduced to 0.93.

2.1.2 Change to longwave water vapour absorption

Calculations of the LW heating rate by water vapour absorption only, without and with the continuum component, from different line-by-line (LbL) models (AER, GFDL, and GLA), show a marked difference between the AER and the two other (older) LbL models, linked to a different and more accurate continuum formulation in the AER LbL model (*Clough et al.*, 1989). *Zhong and Haigh* (1995) (hereafter referred to as ZH) modified an earlier version of the ECMWF longwave code to introduce this new description of the water vapour continuum, from tests with the Oxford GENLIB line-by-line model. The resulting code is more expensive than the operational code due to extra computations of transmission functions. As a trade-off, a revised LW code has been designed which includes fits to the ZH transmission functions but retains as much as possible of the original operational design, so as to minimize the increase in computational time. For the climatological tropical, mid-latitude summer, mid-latitude winter, and sub-arctic winter atmospheres of *McClatchey et al.* (1972) figures 1(a)-(d) show the longwave cooling rate profiles computed by the current operational code, the revised code, the original RRTM code from *Mlawer et al.* (1997) (very close to the AER line-by-line model of *Clough et al.* (1992, 1995)), and the Zhong-Haigh parametrization. The new parametrization corrects the overestimation of the clear-sky cooling in lower layers and produces increased cooling higher up, in much better agreement with the more recent and sophisticated codes.

The coefficients of absorption by the other gases (CO_2, O_3, CH_4, N_2O, CFC11, CFC12), which had been derived from the HITRAN'92 compilation of spectroscopic line parameters, have been checked against the latest HAWKS'96 compilation and found not to require an update. Table 1 compares for the standard atmospheres of McClatchey (TROPical, Mid-Latitude Summer, Mid-Latitude Winter, Sub-Arctic Summer and Sub-Arctic Winter) the outgoing LW

flux (OLR) at the Top of the Atmosphere (TOA) and the surface downward longwave radiation (DLF). For both these quantities the revised LW code is closer to the ZH radiation code than the current operational version.

2.1.3 Change to cloud LW optical properties

The longwave optical properties of ice clouds have been changed from *Smith and Shi* (1992) to *Ebert and Curry* (1992) to ensure a consistent description with the shortwave part of the scheme which also uses a formulation described by *Ebert and Curry* (1992).

Atmos	**OLR** Cntl	**OLR** ZH	**OLR** Pack F	**DLF** Cntl	**DLF** ZH	**DLF** Pack F
TRO	296.8	288.3	292.2	391.9	292.5	392.1
MLS	286.5	278.4	282.0	344.8	346.3	345.0
MLW	233.2	228.2	230.1	218.8	221.2	220.2
SAS	269.0	262.8	265.6	296.1	297.6	296.6
SAW	200.7	197.0	198	167.4	171.2	170.9

Table 1: The clear-sky outgoing longwave radiation (OLR) and surface downward longwave flux (DLF) computed by the operational longwave scheme (Cntl), Zhongh and Haigh scheme (ZH), and the Package F revised scheme (Pack F), for the climatological atmospheres of McClatchey (1972)

2.1.4 Change to the functional relationship between ice effective radius and temperature

Since the radiation code first started to account for ice cloud optical properties with cycle 46 (*Morcrette*, 1994), the ice clouds were assumed to have particles with an effective radius of 40 microns. However observations indicate that the effective radius of ice crystals increases with temperature, usually attributed to accretion on to falling crystals. In the revised scheme, account is taken of this using the diagnostic formulation of *Ou and Liou* (1995).

2.1.5 Change in sea-ice shortwave albedo

For sea-ice, the constant sea-ice albedo of 0.55 is replaced by the parametrization from *Morassutti* (1991), which links the visible and near-infrared albedo to temperature. Sea-ice albedo varies in the range 0.5 to 0.7 as the surface temperature varies between 277.15K and 272.15K, with values being held at 0.5 and 0.7 for temperatures above and below this range respectively. This simple parametrization accounts implicitly for the presence of snow on top of the sea-ice.

2.1.6 Changes to the shortwave radiation scheme

The shortwave (SW) scheme can now be run with either 2 (as in the operational code of Cy18r2 and before) or 4 spectral intervals (1 or 3 in the near-infrared). All radiative properties for gases, water and ice clouds have been recalculated for this enhanced resolution. For clear sky profiles there is very good agreement between the 2 and 4 spectral interval versions of the code. However cloudy sky profiles are more dependent on spectral resolution, indicating that the overlap between the various gases (mainly H_2O and CO_2) and liquid/ice water bands is the main contributor to the effect. The SW optical properties of the current 2-band scheme led to an over prediction of absorption in ice clouds. As spectral resolution is increased (to 4-bands or more) this is reduced. For operational reasons a 2 spectral interval SW scheme is retained, but the cloud optical properties are updated to match those obtained with higher spectral resolution, removing the enhanced absorption found in the current operational scheme.

A treatment of cloud inhomogeneity following *Tiedtke* (1996), in which the cloud water path used in the radiation scheme is multiplied by 0.7, is introduced into the revised shortwave radiation scheme. This contributes to a decrease in both the in-cloud shortwave absorption, and planetary albedo leading to a small increase in downward shortwave radiation at the surface.

2.2 CONVECTION SCHEME

Two aspects of the convection scheme have been modified.

i) *Diagnosis of deep or shallow convection ("Switching")*:

The current operational scheme uses the presence of moisture convergence into a column of the atmosphere due to atmospheric motion to determine whether a point is likely to contain deep or shallow convection. If moisture convergence into a column of the atmosphere is positive then the parameters of the scheme are set to be those appropriate to deep convection. If the opposite is the case then parameters appropriate for shallow convection are used.

In the revised scheme this "switching" has been replaced by one based upon the depth of convection. If the convective cloud depth exceeds 200mb the convection is deemed to be deep, while a cloud with a depth lower than this threshold is treated as shallow convection. The initial depth of the cloud is estimated by an approximate undilute ascent. As this does not included the impact of entrainment or water loading upon the estimation of updraught buoyancy, cloud top height may be overestimated. After a parcel ascent which includes the effects of these processes is calculated, the depth of the cloud is checked again and parameters re-set if a cloud originally assumed to be deep convection only has a depth appropriate to that of shallow convection.

ii) *Deep convective closure*:

Up to the present (Cy18r2 and before) the current operational version of the scheme retains a closure similar to that described in *Tiedtke* (1989). Convective mass flux at cloud base is estimated from the assumption that the moisture (for deep convection) and moist static energy (for shallow convection) of the sub-cloud layer remains constant when convection is active. This has been termed "boundary layer quasi-equilibrium" by *Raymond* (1995). In the revised version of the scheme the estimation of cloud base mass flux for shallow convection remains unchanged. The closure for deep convection is changed to one based upon the concept that convection acts to reduce Convective Available Potential Energy (CAPE) towards zero over a certain timescale (τ). This type of closure is similar to that introduced by *Fritsch and Chappel* (1980) in a mass flux scheme for use in meso-scale models. It has been previously described by *Nordeng* (1994) in tests in an earlier version of the ECMWF model and is further discussed by *Gregory and Nordeng* (1998).

CAPE is defined as

$$\mathrm{CAPE} = \int_{\mathrm{cloud}} g \frac{(\bar{T}_{vl}^{c} - \bar{T}_{vl})}{\bar{T}_{vl}} dz \qquad (1)$$

where superscript "c" refers to the in-cloud values and,

$$T_{vl} = T(1 + 0.608q - l) \qquad (2)$$

with l being the liquid water content of the parcel.

The rate of change of CAPE with time due to convection is

$$\left(\frac{\partial \mathrm{CAPE}}{\partial t}\right)_{\mathrm{conv}} \cong -\int g\left(\frac{\partial \bar{T}_{vl}}{\partial t}\right)_{\mathrm{conv}} dz \tag{3}$$

assuming that the in-cloud properties are constant in time.

Mass flux theory predicts that the effect of convection on large-scale temperature and moisture structures is dominated by compensating subsidence (see for example the study by *Gregory and Miller*, 1989). Neglecting the effect of convection on the large-scale water content of the atmosphere and ignoring the contribution of the grid-box mean water content to virtual temperature, eqn(3) can be expressed as

$$\left(\frac{\partial \mathrm{CAPE}}{\partial t}\right)_{\mathrm{conv}} \cong -\int g M_c \left((1+608\bar{q})\frac{\partial \bar{T}}{\partial z} + 0.608\bar{T}\frac{\partial \bar{q}}{\partial z}\right) dz \tag{4}$$

M_C, the cloud mass flux, accounts for both updraught and downdraught mass fluxes. Expressing this as a combination of the mass flux at the base (M_B) of the updraught and top (M_T) of the downdraught, together with functions (η) which describe the variation of the mass fluxes with height (derived from the entraining/detraining plume model of convection),

$$M_c = M^{UD} + M^{DD} = M_B^{UD}\eta^{UD} + M_B^{DD}\eta^{DD} \tag{5}$$

The initial mass flux at the top of the downdraught is taken to be proportional to the mass flux at the base of the updraught,

$$M_T^{DD} = -\alpha M_B^{UD} \tag{6}$$

where α is 0.3. Then eqn (6) can be rearranged as

$$M_C = M_B^{UD}(\eta^{UD} - \alpha\eta^{DD}) \tag{7}$$

Assuming that convection acts to reduce CAPE towards zero over a timescale τ

$$\left(\frac{\partial \mathrm{CAPE}}{\partial t}\right)_{\mathrm{conv}} \cong -\frac{\mathrm{CAPE}}{\tau} \tag{8}$$

substitution of eqns (7) and (8) into eqn (4) gives after rearrangement an expression for the mass flux at the base of the updraught;

$$M_B^{UD} = \frac{\left(\frac{\mathrm{CAPE}}{\tau}\right)}{\int g(\eta^{UD} - \alpha\eta^{DD})\left((1+0.608\bar{q})\frac{\partial \bar{T}}{\partial z} + 0.608\bar{T}\frac{\partial \bar{q}}{\partial z}\right) dz} \tag{9}$$

As the downdraught mass flux is related to that of the updraught by eqn (6), eqn (9) allows the estimation of the intensity of the convection to be calculated.

Nordeng (1994) discusses the choice of the timescale τ. He argues that it must be such that convection is able to come into equilibrium with large-scale ascent while maintaining realistic temperature and moisture structures. Here an adjustment timescale of 2 hours is chosen for T63 resolution simulations. Experience suggests that the magnitude of the

resolved vertical motion roughly doubles with as horizontal resolution is halved. The adjustment timescale is therefore varied linearly with resolution, being (63/213) x 2 hours for simulations at T213 resolution.

In seasonal simulations at T63 the revised convection scheme has a large impact upon the simulated distribution of tropical precipitation (not shown) bringing may features into closer agreement with observed climatologies. In particular a weaker, broader ITCZ is found over the Atlantic and Pacific oceans in both northern winter and summer. Over India during June/July/August the rainfall pattern is more continuous while during December/January/February rainfall in the equatorial west Pacific is increased. As will be seen later these changes are similar to those seen in the combined package (figs 2 and 12).

2.3 CLOUD SCHEME

The fallout of cloud ice in the model is governed by the equation

$$\frac{\partial l}{\partial t} = \frac{1}{\rho}\frac{\partial}{\partial z}(\rho v_i l) \tag{10}$$

where v_i is the terminal fallspeed of the ice particles and l is the cloud ice content. A spatial discretization of this equation for layer k can be written as

$$\left(\frac{\partial l}{\partial t}\right) = \frac{(v_i l)^{k-1} - (v_i l)^k}{\Delta z} \tag{11}$$

where for simplicity we assumed a constant density (ρ). Besides the prognostic ice variable the model also has a diagnostic snow variable. Currently (Cy18r2 and earlier) it is assumed that all ice leaving model layer k is converted into snow and therefore falls to the surface in the same timestep, evaporating as it falls through lower layers of the model. In terms of equation (11) this is equivalent to assuming that $(v_i l)^{k-1} = 0$. This treatment introduces an undesirably strong dependence on vertical resolution in equation (11).

Originally (experimental cloud scheme in Cy11r7) equation (11) was integrated in time analytically giving the solution

$$l^k(t+\Delta t) = l^k(t)e^{(-D\Delta t)} + \frac{C}{D}(1 - e^{(-D\Delta t)}) \tag{12}$$

with

$$C = \frac{(v_i l)^{k-1}}{\Delta z}$$

and

$$D = \frac{v_i^k}{\Delta z}$$

This solution is applied to all ice falling into cloud in the layer below whereas for ice falling into clear sky a conversion into snow as above is assumed. The better numerical treatment of eqn(12) was removed before the operational implementation of the cloud scheme due to a large positive temperature bias in the Tropics caused by the interaction of

the much larger cloud ice amounts with the radiation. Allowing falling ice to be converted immediately into snow led to a considerable reduction in cloud ice content leading to smaller temperature biases.

As discussed in section 2.1.6 an inconsistency has been found in the radiation scheme that led to anomalously high solar absorption in cloud which contributed strongly to the warm bias in the Tropics. After removing this inconsistency the possibility of reintroducing the formulation of eqn(12) for ice fallout has been tested. *Klein and Morcrette* (1997) showed that the larger ice contents produced by the new formulation are much more realistic when compared to observations in the case of a cirrus cloud observed during FIRE II. Other comparisons to observations (CEPEX, ICE) have also shown that the cloud ice content of the current model is too small sometimes by a factor of 2 or more. Based on this evidence the change back to the original formulation was introduced in PACKAGE F leading to an improved representation of cloud ice content without any negative impact on the temperature biases (see section 3 below).

2.4 VERTICAL DIFFUSION SCHEME

The vertical diffusion scheme is now called three times within each model timestep, improving the accuracy of the surface drag coefficient. In T213 forecasts coupled to the wave model this gives improved performance which will be reported on in a forthcoming report.

3. IMPACT ON MODEL CLIMATE IN SEASONAL FORECASTS

Much of the motivation for the introduction of the revised physics package came from a desire to improve model performance in seasonal forecasting where climate drift is an important issue. The performance of the coupled ocean-atmosphere version of the IFS used to make forecasts on seasonal timescales is sensitive to the tropical circulation and associated diabatic heating, together with fluxes of energy at the surface and the Top of Atmosphere (TOA).

Ensembles of T63 simulations are used to assess the impact of the revised physics package upon the seasonal climatology of the model for June/July/August 1987 (JJA87) and December/January/February 1987/88 (DJF8788). The series of experiments are named;

June/July/August 1987	: CONTROL	: ZQ3T
	: PACKAGE F	: ZPSD
December/January/February 1987/88	: CONTROL	: ZPF8
	: PACKAGE F	: ZPSC

These experiments were performed with Cy16r2 of the IFS with an additional correction to the formulation of convective momentum transports (discussed by Gregory, 1997) included. Estimates of the model's seasonal climate for these periods were obtained by averaging over three simulations, each using the observed sea surface temperature (SST) and starting 1 day apart. For JJA87 initial dates were 29/04/87, 30/4/87 and 1/5/87, while for DFJ8788 they were 30/10/87, 31/10/87 and 1/11/87, all simulations being 125 days in length. All the results discussed below are ensemble averages for the periods indicated.

3.1 JUNE/JULY/AUGUST 1987

Changes to the precipitation patterns are broadly similar to those associated with the convection scheme alone (not shown). Comparison of the tropical rainfall in the control (fig 2b) and PACKAGE F (fig 2c) simulations with the GPCP precipitation climatology (fig 2a) show that the revised parametrizations bring the model's climate into better agreement with observations. Improvements include a weaker ITCZ north of the equator over the Pacific and Atlantic oceans. Precipitation amounts over northern S.America are increased, while being reduced over equatorial Africa, although they are still wetter than in the GPCP climatology near Lake Chad. Substantial improvements are seen in the Indian Monsoon

region where the area covered by precipitation rates greater than 5mm/day is more continuous, with excessively dry regions over India and the Philippines being corrected. The rainfall amounts over the Ghats along the western side of India are also improved.

Associated with a reduction in the peak intensity of precipitation along the ITCZ, the magnitude of zonal mean vertical ascent in the tropics is reduced in the PACKAGE F simulation (fig 3c) compared to the control (fig 3b), in better agreement with ECMWF Re-Analysis (ERA) estimates (fig 3a). Excessive vertical motion in the lower troposphere is reduced while the depth and latitudinal extent of the Hadley circulation is also better captured. However the intensity of the ascending branch is still too weak compared to ERA estimates in the upper troposphere. Errors in zonal mean meridional wind (not shown) in the outflow region of the Hadley cell are reduced by 50% in the PACKAGE F simulations.

The improved pattern of diabatic heating in the tropics with PACKAGE F leads to an improvements in the simulated 850hPa winds in the tropics and sub-tropics. Comparison of the flow from the control (fig 4a) and PACKAGE F (fig 4c) simulations with ERA (fig 4b) show that excessive cross equatorial meridional flow in the control simulation is reduced with PACKAGE F in both the Atlantic and Pacific, in better agreement with ERA. However wind strength in the trade wind regions is still slightly over estimated. Over equatorial west Africa, the low level flow is much weaker with PACKAGE F, consistent with the reduction in rainfall amounts, and again in better agreement with ERA. However to the east of Lake Chad, the northerly flow over the Sahara is still too weak while the westerly flow to the south is too strong.

In the monsoon region over the Indian sub-continent and surrounding oceans the flow is better captured. Over the Arabian Sea the intensity of the low level jet is increased and penetrates further northward. Over S.E. Asia the monsoon jet extends further to the east, in agreement with ERA. Flow to the east of the Philippines is more easterly with PACKAGE F, reducing biases seen in the control simulation. Changes in the 200hPa tropical flow are less apparent with the revised physics, although in the zonal mean easterly errors in the upper troposphere between 0 and 30°S are reduced from -2ms^{-1} to zero (not shown).

Differences between control and PACKAGE F simulations from ERA zonal mean temperature are shown in fig 5a. Temperature biases in the upper tropical troposphere in the control simulation (fig5a(ii)) are reduced by PACKAGE F (fig 5b(iii)), although increased in the lower stratosphere (a direct radiative effect due to the increased cloud cover and water contents in the tropical upper troposphere). At low levels the revised continuum in the radiation scheme removes the cold bias seen in the control simulation in the tropics and both northern and southern hemisphere mid-latitudes (although here a warm bias is seen with PACKAGE F). Cold biases in the vicinity of the tropopause in mid-latitudes are slightly increased with the revised physics. This is mainly due to the removal of excessive solar absorption in clouds and is compensated somewhat by the inclusion of the revised ice precipitation treatment which gives increased cloudiness and water contents in the upper troposphere (see figures 6 and 7 later). Experiments with the revised radiation scheme alone (not shown) gave a reduced cold bias in the lower troposphere compared to the physics of the control simulation of a similar magnitude to that with PACKAGE F, but produced more substantial cooling in the upper troposphere of the mid-latitudes.

Considering the zonal mean mixing ratio compared to ERA data (fig 5b), PACKAGE F (fig 5b(iii)) moistens the tropics between 10S and 20N. This is caused by both the changes to the convection scheme and ice precipitation treatment. In the boundary layer the dry bias seen in the control simulation (fig 5b(ii)) is reduced. However the overall moistening of the deep tropics with PACKAGE F leads to an increase in the mid-tropospheric moisture bias, with a moisture excess over ERA values of 0.5g/kg in the control simulation increasing to 1g/kg. PACKAGE F has little impact upon the intensity or depth of the dry bias of the lower troposphere in the sub-tropics of either hemisphere.

The pattern of upper level cloudiness in the model is affected by the revised parametrizations. Cloud amount (fig 6) increases in the upper troposphere when PACKAGE F is used (fig 6c c.f fig 6b) as do cloud water/ice contents (fig 7c c.f. fig 7b). In mid-latitudes this is mainly due to the revised ice fallout, although in the tropics the revised convection scheme also contributes. As noted above (section 2.3) the revised ice fallout scheme gives ice water contents which are in better agreement with the few observations available. Figure 8 compared the spatial pattern of cloudiness in the control

(fig 8b) and PACKAGE F (fig 8c) simulations with ISCCP estimated (fig 8a). Cloud cover is increased in many regions in the tropics with PACKAGE F. In the Indian monsoon region the area covered by cloud amounts greater than 65% is increased, in better agreement with observations. However the extent of regions with cloudiness above 80% is too large with PACKAGE F compared to ISCCP estimates. In the sub-tropical regions over the Pacific and Atlantic total cloud amount is slightly increased.

The increased cloud fractions and more realistic distribution of precipitation that PACKAGE F provides lead to reduced errors in top of atmosphere (TOA) radiative fluxes when compared to ERBE data. Over estimates of OLR (fig 9 - negative values shaded) seen in the control simulation (fig 9b) over India and S.E Asia, Africa and northern S.America are greatly reduced with PACKAGE F (fig 9c) leading to better comparison with ERBE OLR estimates (fig 9a). However in some regions (for example along the Pacific ITCZ) OLR is underestimated with PACKAGE F, providing further evidence that tropical high cloud amounts may be too large in these regions as indicated by comparison with ISCCP data (although the radiative optical properties scheme and cloud water/ice contents may play a role). Biases in the northern hemisphere of the control simulation (fig 9b) are also reduced by PACKAGE F (fig 9c), a consequence of the revisions to the long wave radiation scheme described above (section 2.1 above).

Errors in the estimation of TOA incoming flux of shortwave radiation in the tropics and sub-tropics of the control simulation (fig 10b - negative values indicating an over estimation of albedo) are slightly reduced by PACKAGE F (fig 10c), specifically along the Pacific ITCZ and the sub-tropics of the Pacific and Atlantic oceans. The treatment of the inhomogeneity of clouds in PACKAGE F tends to reduce excessive albedos seen in the control simulation but this is counter balanced to a great extent increased high level cloudiness. In northern mid-latitudes, the PACKAGE F simulation has too large an TOA incoming shortwave flux compared to ERBE, the error increasing over that found in the control simulation. Although high cloud cover is increased in these regions by the changes in PACKAGE F, the inclusion of an effective radius which increases with temperature reduces the albedo of these mid-latitude clouds from that in the control simulation.

Of importance to coupled ocean-atmospheric models is the net surface heat flux. Figure 11 shows the zonal mean ocean net surface heat flux from control and PACKAGE F simulations of JJA87, together with values from the observed climatology of *da Silva* (1994). Between 30°N and 60°S, PACKAGE F is in closer agreement with the climatology, increases in surface heating coming manly from increased solar radiation at the surface together with a smaller contribution from a reduction in surface evaporation. This corrects a surface cooling bias in the control simulations and should contribute to correcting a cold bias of SST in the tropics seen in coupled ocean-atmosphere simulations with the control physics (see section 5, footnote 1). However north of 60°N, due to reduced TOA albedo in the PACKAGE F simulation (indicated in figure 10c) and so increased surface downward shortwave radiation, the over estimation of the net surface flux already present in the control simulation is increased with PACKAGE F.

3.2 DECEMBER/JANUARY/FEBRUARY 1987/88

Figure 12 compares simulated precipitation for DJF 1987/88 from the control (fig 12b) and PACKAGE F (fig 12c) simulations with observed estimates from GPCP (fig 12a). As for the northern summer months, precipitation changes for DJF 1987/88 brought about by the revised physics are broadly similar to those caused by the revisions to the convection scheme alone (not shown). With PACKAGE F the intensity of the Pacific ITCZ is reduced and greater rainfall occurs on the equator in the west Pacific, although amounts ate still under estimated there. The maximum rainfall in this region remains north of the equator associated with an over active depression track. Rainfall is increased along the north and east coasts of Australia, to the east of the date line and the South Pacific Convergence Zone (SPCZ) extends further into the southern hemisphere. All these changes brought about by PACKAGE F bring the simulated rainfall pattern into better agreement with the GPCP climatology than in the control simulation. However over south America the rainfall is reduced in the PACKAGE F simulation, the resulting amount being lower than in the climatology.

As for northern hemisphere summer, zonal mean average vertical velocity (not shown) indicates that the ascending branch of the Hadley circulation becomes weaker, broader and slightly deeper with PACKAGE F, in better agreement with ERA data. Errors in zonal mean meridional wind in the upper tropical troposphere are also reduced. The upper level

zonal flow in the tropics is more affected by the changes to the physics in DJF than JJA. Figure 13 shows the zonal mean of the zonal wind from the control (fig 13b) and PACKAGE F (fig 13c) simulations differenced against ERA data (fig 13a). The PACKAGE F simulation shows substantially reduced easterly errors in the upper troposphere of the tropics. A maximum easterly errors in the control simulation of -7m/s between model levels 10 and 5 is reduced to near -2m/s in PACKAGE F. This reduction in the easterly bias in upper levels is associated with the improved distribution of tropical precipitation and increased upper level cloud cover resulting from the revised treatment of the fallout of cloud ice. In the east Pacific, westerly flow in the upper troposphere (important for tropical-extratropical interactions) is better captured with PACKAGE F (not shown). Errors in zonal wind are also reduced in the mid-latitudes of the northern and southern hemisphere in the PACKAGE F simulations, although due to variability in these regions an ensemble of three simulations may be inadequate to provide a signal which is significant.

Figure 13c also shows that errors in the low level zonal wind are reduced between the equator and 30°N in the PACKAGE F simulation compared to the control integration. This is associated with reduced easterly flow over the Atlantic and Pacific as indicated by the 850hPa wind field, shown in fig 14 for the control (fig 14a) and PACKAGE F (fig 14c) simulations, together with ERA data (fig 14b). With the improved precipitation patterns over the west Pacific with PACKAGE F, errors in the low level flow in these regions are reduced. North of New Guinea a predominately meridional flow with the control physics package is replace by an easterly flow with PACKAGE F, as found in ERA. The westerly jet north of Australia, associated with the Australian monsoon, absent in the control simulation, is captured in the PACKAGE F simulations although the strength of the flow is underestimated compared to ERA estimates.

Changes to the temperature and moisture fields of the model by PACKAGE F are similar to those described for JJA87 discussed above. For temperature (fig 15) cold biases in the low levels of the model in the control simulation (fig 15b) are reduced with the introduction of PACKAGE F (fig 15c). Cloud amounts and water contents (not shown) are increased in the upper troposphere, especially in the tropics. Bias in TOA fluxes of OLR and net incoming shortwave radiation (against ERBE data) in the tropics and sub-tropics are reduced in a similar manner to JJA87. However errors in the shortwave flux over the winter (southern) hemisphere storm track are worse in the PACKAGE F simulation (not shown), associated with the temperature dependency of the effective radius of ice particles introduced into the cloud radiative optical properties scheme.

4. IMPACT ON MEDIUM-RANGE FORECASTS

Two series of analysis/forecast experiments were carried out using PACKAGE F in conjunction with an experimental version of the 4D-Variational analysis system in order to assess the impact of the revised physics package on medium-range forecast performance using the T213 version of the IFS;

from 19970115-19970130	: CONTROL (Cy16r3)	: ZQ0L
	: PACKAGE F (Cy16y3+Mod. Physics)	: ZQID
from 19970901-19970930	: CONTROL (Cy16r4)	: ZQLA
	: PACKAGE F (Cy16r4+Mod. Physics)	: ZQPY

Verification is carried out against the operational analyses for the periods in question, which were created using a 3D-Variational analysis system. However tropical wind scores are presented verified against an experiments own analysis, i.e. from the 4D-Var analysis system. In order to consider the most representative results (often difficult with a small number of experiments), scores are averaged over both periods (last half of January and September 1997) unless otherwise stated - a total of 38 cases being used (16 from January 1997 and 22 from September 1997). This is less than the total number of forecasts carried out due to the difficulties in archiving data.

At 500hPa both anomaly correlation (AC) and root mean square error (RMSE) indicate the impact of PACKAGE F on model performance over the northern hemisphere (fig 16a) and Europe (fig 16b) is neutral. In the southern hemisphere

AC is smaller (RMSE slightly larger) with PACKAGE F after day 4. Scatter plots of 500hPa height for these regions (figure 17) show relatively little scatter out to 120 hours, confirming that the signals seen in the mean scores are robust. For the southern hemisphere (fig 18b) the negative impact of PACKAGE F is caused by 2 poor forecasts only (1 each from the January and September period).

Figure 18 shows the 850hPa mean temperature error through the forecast for the northern (fig 18a - top panel) and southern hemispheres (fig 18a - bottom panel). As seen in the seasonal simulations above, PACKAGE F reduces the cold bias of the control physics package at 850hPa, by around 0.5K in the northern hemisphere and 0.25K in the southern hemisphere. In the southern hemisphere the temperature bias is relatively constant throughout the 10 day forecast period with PACKAGE F. This is in contrast with the signal in the northern hemisphere where the a growing cold bias with the control physics package through the first 5 days of the forecasts is replaced with PACKAGE F by a warm bias which grows steadily through the forecast period. At 200hPa in both the northern (fig 18b - top panel) and southern (fig 18b - bottom panel) hemispheres a near constant temperature bias through the forecast with the control physics is replaced by a cooling trend with PACKAGE F, leading to a cold bias of the model of -0.5K at the end of the 10 day forecast period.

Zonal mean cross sections of day 5 temperature errors as measured against an experiments own analysis are shown in figure 19a for the control physics and figure 19b for PACKAGE F. These have been calculated from 15 cases from September period and show a similar signal to that seen in the hemispheric mean score of figures 18a and b, and also the seasonal simulations discussed in section 3 above. In the mid-latitudes of both the northern and southern hemisphere the lower troposphere is warmed by PACKAGE F (fig 19c showing the difference between PACKAGE F and the control physics). This results in a reduction of a low level cold bias in the southern hemisphere between 30 and 50S seen in the control forecasts. In the mid-latitudes of the northern hemisphere, the low level warming tendency of PACKAGE F corrects the cold bias in the control forecast between 20 and 40N but leads to an increased low level warm bias centred around 60°N. Slight increases in cold bias are seen in the upper troposphere of the mid-latitudes with PACKAGE F, while in the tropics, biases in both upper and lower troposphere are reduced by PACKAGE F.

The performance model in the medium-range is very sensitive to nature of the temperature simulation in the upper troposphere of the mid-latitudes. As discussed in section 3 above, the tendency of the revised radiation scheme of PACKAGE F to cool the upper troposphere is compensated in the mid-latitudes by the revised treatment of ice precipitation, which increases cloud cover and water content in the upper troposphere leading to a greater absorption of long wave radiation emitted from the lower troposphere. Experiments with the revised radiation scheme alone (not shown) led to a larger cooling of the upper troposphere, resulting in a degradation of the medium-range forecast performance of the model in the mid-latitudes. Approximate calculations indicate that this is caused by a decreased static stability of the mid-latitude atmosphere leading to increased baroclinic instability growth rates and eddy kinetic energy.

Differences of day 5 zonal mean mixing ratio (on pressure levels) from operational analyses are shown in figure 20. As for the temperature biases of figure 19, these are averages over 15 cases from the September period. With the control physics (fig 20a) the forecasts show a dry bias up to 600hPa between the equator and 50N. South of the equator there is a low level dry bias between the equator and 40S, typically extending up to 800hPa. With PACKAGE F (fig 20b), dry bias of the model in both northern and southern hemispheres is generally restricted to below 900hPa. However above this level some regions (around 20°N and 0-20°S) show a moist bias, the maximum moisture excesses being found near 800hPa. Figure 20c shows the difference in mixing ratio between forecasts using PACKAGE F and the control physics package, showing a moistening of the troposphere above 900hPa north of the equator. Below 900hPa, between the equator and 30°N, PACKAGE F tends to increase the dry bias of the model.

The changes in the moisture bias of the forecasts between those using the control and PACKAGE F parametrizations are somewhat different those changes seen in seasonal simulations discussed in section 3. There (figure 5b - JJA 1987), while a deep dry bias was seen in the control simulation compared to ERA (fig 5b(ii) - middle panel), this was only reduced in the deep tropics. The bias in the sub-tropics was little affected by the changes to the physical parametrizations of PACKAGE F. This may reflect that the moisture changes seen between the seasonal simulations using the control and PACKAGE F physics reflect an adjustment to new model tropical climate, while after 5 days the moisture field of the model in the tropics and sub-tropics may not have reached such new equilibrium. However direct comparison of the

moisture fields between the seasonal and medium-range forecasts is difficult due to the different times of annual cycle the simulations represent.

The impact of the revised physics package upon forecast winds is shown in figure 21, where RMSE winds errors (as measured against operational analyses) at 850 (fig 21a) and 200hPa (fig 21b) for northern and southern hemispheres are plotted. At both of these pressure levels there is a marginal increase in RMSE in both the northern and southern hemispheres with the use of PACKAGE F. Because tropical winds are sensitive to the nature of the diabatic heating provided by parametrized processes, it is often difficult to assess the impact of a modified physics package against an analysis which is created using a different parametrizations. The impact of PACKAGE F upon tropical winds is therefore assessed using RMSE wind errors measured against a forecasts own analysis over the first 3 days of the forecast period. Figure 22 shows 850 and 200hPa RMSE wind errors for the tropics, averaged for the 15 September forecasts used in figure 19 and 20, for the control and PACKAGE F forecasts. As in the seasonal simulations errors at 850hPa are reduced. However at 200hPa wind errors are slightly increased with PACKAGE F. In the seasonal simulations the flow at this level during northern summer was little affected by PACKAGE F, while an easterly bias was reduced during northern winter. The disparity between these signals and that of in the short-range forecasting period may be due to the different times in the annual cycle that the forecast are made.

Figure 23 shows the evolution of globally averaged precipitation and surface evaporation through a 10-day forecast (averaged over 14 cases from the September period) for the control physics (fig 23a) and PACKAGE F (fig 23b). Both evaporation and precipitation rates are increased with PACKAGE F. There is also an increase in the spin-down of precipitation in the first 24 hours with the revised physics package. As found in T63 seasonal simulation the pattern of precipitation is also changed by the revised physics package. With the control physics package, through a 10 day forecast it is common for the intensity of rainfall in the ITCZ of the tropical Pacific to increase through the simulation. Figure 24 compares the average day 10 rainfall for the February period from the control (fig 24a) and PACKAGE F experiments (fig 24b). With the revised physics package rainfall rates are reduced along the Pacific ITCZ, in a similar manner to that found in the seasonal simulation (fig 12). Other precipitation changes with PACKAGE F are similar to those seen in T63 simulations, with the area covered by rainfall rates greater than 5mm/day being increased over the west Pacific and in the South Pacific Convergence Zone (SPCZ) and rainfall amounts being reduced over Africa and South America. Overall tropical precipitation pattern are less noisy with the revised physics. Study of individual forecasts suggests smoother 24 hours average precipitation patterns over the north Atlantic also.

5. SUMMARY

A set of modifications to the physical parametrizations of the ECMWF IFS has been described and their impact upon both seasonal and medium forecasts discussed.

The climatology of seasonal simulations has been improved, major changes being;

a) Clear sky radiative fluxes at the top the atmosphere and at the surface have been improved. "Anomalous absorption" of short wave radiation by clouds due to spectral truncation has been eliminated. The ocean surface energy budget is closer to climatological estimates in the tropics and sub-tropics, which should result in improved Sea Surface Temperatures (SSTs) in coupled atmosphere-ocean experiments.

b) The revised convection scheme improves the distribution of tropical precipitation with the intensity of the ITCZ in both Pacific and Atlantic being reduced. Tropical winds are improved in the Indian Ocean and Pacific in both the upper and lower troposphere. The magnitude of the zonal mean vertical velocity in the ascending branch of the Hadley circulation is weakened and the latitudinal extent of the ascending branch widened

c) The change to the ice fall out formulation increase both upper level cloud and ice water content amounts. Although the ice content of the atmosphere is not well observed, previous studies (*Rizzi and Jakob*, 1996) have suggested that the current ice fall out formulation leads to an underestimate of the ice water amounts. Study of a well documented FIRE case (*Klein and Morcrette*, 1997) indicates that the increased ice water contents with PACKAGE F are in better agreement with observed amounts.

These changes to the climatology of the model should results in improved SST forecasts in coupled atmosphere-ocean simulations[1]. The climatology of AMIP simulation carried out using the IFS should also be improved.

Analysis-forecast experiments have been carried out using an experimental version of the 4D-Variational analysis system. The impact of the package is generally neutral averaged over January and September 1997 periods. However tropical temperature biases are reduced in both the upper and low troposphere while a low level cold bias is reduced in the mid-latitudes. A clear signal with the revised convection scheme is the removal of the spin-up of the ITCZ through a 10-day forecast, a signal which has been noted for some time in the operational model. Given both the improved simulation in both aspects of seasonal and medium-range forecasts, PACKAGE F was introduced into the operational version of the IFS at ECMWF on the 16th of December 1997.

As noted in the introduction, the study illustrates the methodology by which changes to model physics are implemented into the ECMWF IFS. Two points of general interest to the wider community working to improve NWP and climate models are highlighted. Firstly the use of seasonal simulations together with higher resolution forecasts out to the medium range proves valuable in assessing the impact of the revisions to the models physics package. Many of the changes seen in the seasonal simulations (for example changes to temperature and precipitations patterns) were also found in the medium-range forecasts. Since tests with a data assimilation/forecasts system are generally more expensive and complex than carrying out an ensemble of seasonal forecasts, the later provide a relatively efficient method by which the impact of model changes can be efficiently assessed. However the data assimilation/forecast tests also highlighted difficulties which were not apparent from seasonal simulations alone.

As noted in section 4 above, in an early version of the revised physics package (with the convection and radiation changes alone) more intense upper tropospheric cooling resulted compared to the control forecasts. As a result, due to an increase in eddy kinetic energy in the mid-latitude storm tracks, scores in the 5 to 7 day range were lower than those of the control forecasts. However the seasonal simulations were relatively insensitive to this aspect of the revised physics, the seasonal climatology of the model in the mid-latitudes being little changed. This may be due to the scales involved in the development of baroclinic eddies being less well resolved at T63 than T213, but also the variability of the mid-latitudes found in seasonal forecasts may mask any signal. The use of high resolution medium range forecasts is particularly beneficial for considering the impact of model changes upon mid-latitude flow as due to the highly variable nature of these regions it is often difficult to identify signals caused directly by physics changes without running a large ensemble of seasonal forecasts. The use of both medium-range and seasonal forecasts contrasts with many studies considering the impact of physical parametrizations upon model performance in which only seasonal or multi-year simulations are considered.

To compensate for the upper tropospheric cooling caused by the reduction in cloud short wave absorption and the revised continuum in the PACKAGE F radiation scheme, the improved treatment of ice precipitation was added to the package, helping to maintain forecast performance in the medium range through a compensating warming in the upper levels due to increased cloud amounts and water contents. This illustrates a second important point. Each of the components of the package was evaluated in single column model and/or case studies against observational and high resolution model data. While all improved aspects of model performance, when introduced individually into full ECMWF model each alone did not bring an overall improvement in model performance. Deficiencies in other parts of the models parametrization package may contribute to a worsening of performance, and interactions between different components of the models parametrizations need to be taken into account. Thus rather than introducing changes to an single parametrization it is often necessary to introduce a combined set of changed parametrizations together. This points to the uncertainty which

1. Initial coupled ocean-atmosphere simulations indicate that ocean surface temperature bias over a large part of the tropics are reduced by PACKAGE F, although sea surface temperature errors increase in the vicinity of stratocumulus sheets and in the southern hemisphere depressions track. Considering averages over forecasts started from difference times of the year the ability of the revised model to predict sea surface temperature anomalies appears to be slightly increased. (Stockdale, personal communication).

continues to exist over the parametrization of physical processes in large-scale models of the atmosphere and especially their interaction with one another. Such uncertainty will only be reduced through further studies of the processes involved using a combination of observational data and high resolution models of the processes concerned.

6. REFERENCES

Clough, S.A., F.X. Kneizys, and R.W. Davies, 1989: Line shape and the water vapor continuum., Atmos. Res., **23**, 229-241

Clough, S.A., M.I. Iacono, and J.-L. Moncet, 1992: Line-by-line calculations of atmospheric fluxes and cooling rates: Application to water vapor., J. Geophys. Res., **97D**, 15761-15786.

Clough, S.A., and M.I. Iacono, 1995: Line-by-line calculation of atmospheric fluxes and cooling rates: 2 - Application to carbon dioxide, ozone, methane, nitrous oxide and the halocarbons., J. Geophys. Res., **100D**, 16519-16536

da Silva, A.M., Young, C.C. and Levitus, S., 1994: Atlas of surface marine data., US Dept. of Commerce, NOAA, Washington

Ebert, E.E., and J.A. Curry, 1992: A parametrization of ice cloud optical properties for climate models., J. Geophys. Res., **97D**, 3831-3836

Gregory, D., 1997: Correction of coding error in formulation of convective momentum transport parametrization., ECMWF Research Department Memorandum, ECMWF, Shinfield Park, Reading, Berks, United Kingdom, July 1997

Gregory, D. and Miller, M.J., 1989: A numerical study of the parametrization of deep tropical convection., Q. J. R. Meteorol. Soc., **115**, 1209-1241

Gregory, D. and Nordeng, T.E., 1998: Characteristics of instability and moisture convergence based closures in the ECMWF mass flux convection scheme. Part 1: Single Column Model studies., In preparation

Klein, S. and Morcrette, J.-J., 1997: Simulation of a cirrus cloud observed during the FIRE-II field experiment., ECMWF Research Department Memorandum, ECMWF, Shinfield Park, Reading, Berks, United Kingdom, August 1997

Kondraty'ev, K. Ya., 1972: Radiation processes in the atmosphere., Second Lecture, WMO-309, Geneva, 214 pp

Masuda, K., T. Takashima, and Y. Takayama, 1988: Emissivity of pure and sea waters for the model sea surface in the infrared window region., Remote Sensing Environment, **24**, 313-329

McClatchey, R.A., R.W. Fenn, J.E.A. Selby, F.E. Volz, and J.S. Garing, 1972: Optical properties of the atmosphere., AFCRL-72-0497, Bedford, Mass., Environm. Res. Pap. 411, 3rd ed., 108 pp

Morassutti, M.P., 1991: Climate model sensitivity to sea ice albedo parameterization., Theoret. Appl. Climatol., **44**, 25-36

Morcrette, J.-J., 1993: Revision of clear-sky and cloud radiative properties in the ECMWF model., ECMWF Newsletter, **61**, 3-14

Nordeng, T.E., 1994: Extended versions of the convection parametrization scheme at ECMWF and their impacts upon the mean climate and transient activity of the model in the tropics., Research department technical Memorandum No. 206, ECMWF, Shinfield Park, Reading, Berks, United Kingdom

Raymond, D.J., 1995: Regulation of moist convection over the west Pacific warm pool. Journ. Atm. Sci., **52**, 3945-3959

Rees, W.G., and S.P. James, 1992: Angular variation of the infrared emissivity of ice and water surfaces., Intern. J. Rem. Sens., **13**, 2873-2886

Rees, W.G., 1993: Infrared emissivities of Arctic land cover types., Intern. J. Rem. Sens., **14**, 1013-1017

Rees, W.G., 1993: Infrared emissivity of Arctic winter snow., Intern. J. Rem. Sens., **14**, 3069-3073

Rizzi, R. and Jakob, C., 1996: Evaluation of model OLR in cloudy regions using TOVS 1b data., ECMWF Research Department Memorandum, ECMWF, Shinfield Park, Reading, Berks, United Kingdom, December 1996

Taylor, S.E., 1979: Measured emissivity of soils in the Southeast United States., Remote Sens. Environm., **8**, 359-364

Tiedtke, M., 1989: A comprehensive mass flux convection scheme for cumulus parametrization in large-scale model., Mon. Wea. Rev., **117**, 1779-1800

Tiedtke, M., 1996: An extension of cloud-radiation parameterization in the ECMWF model: The representation of sub-grid scale variations of optical depth., Mon. Wea. Rev., **124**, 745-750

van de Griend, A., M. Owe, M. Groen, and M. Stoll, 1989: Measurement and spatial variation of thermal infrared surface emissivity in a savanna environment., Water Resource Res., **27**, 371-379

Zhong Wenyi, and J.D. Haigh, 1995: Improved broadband emissivity parameterization for water vapor cooling rate calculations., J. Atmos. Sci., **52**, 124-138

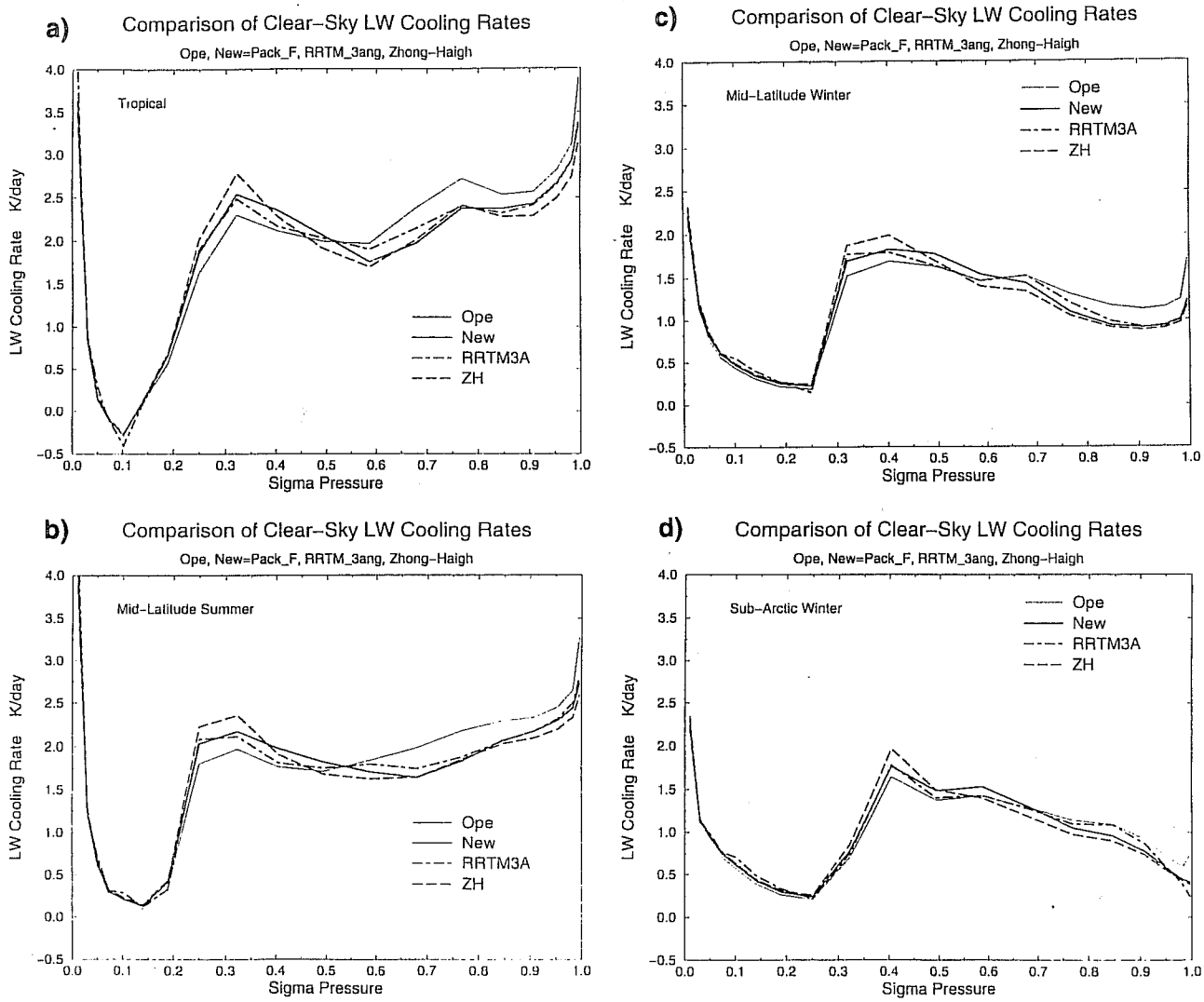

Fig. 1 Comparison of clear sky radiative cooling rates for (a) tropical profile, (b) Mid-latitude summer, (c) Mid-latitude winter and (d) Sub-Arctic winter for the operational LW code (Ope), the revised LW code (New - as in PACKAGE F), the rapid radiative transfer model (RRTM) and Zhong and Haigh LW code.

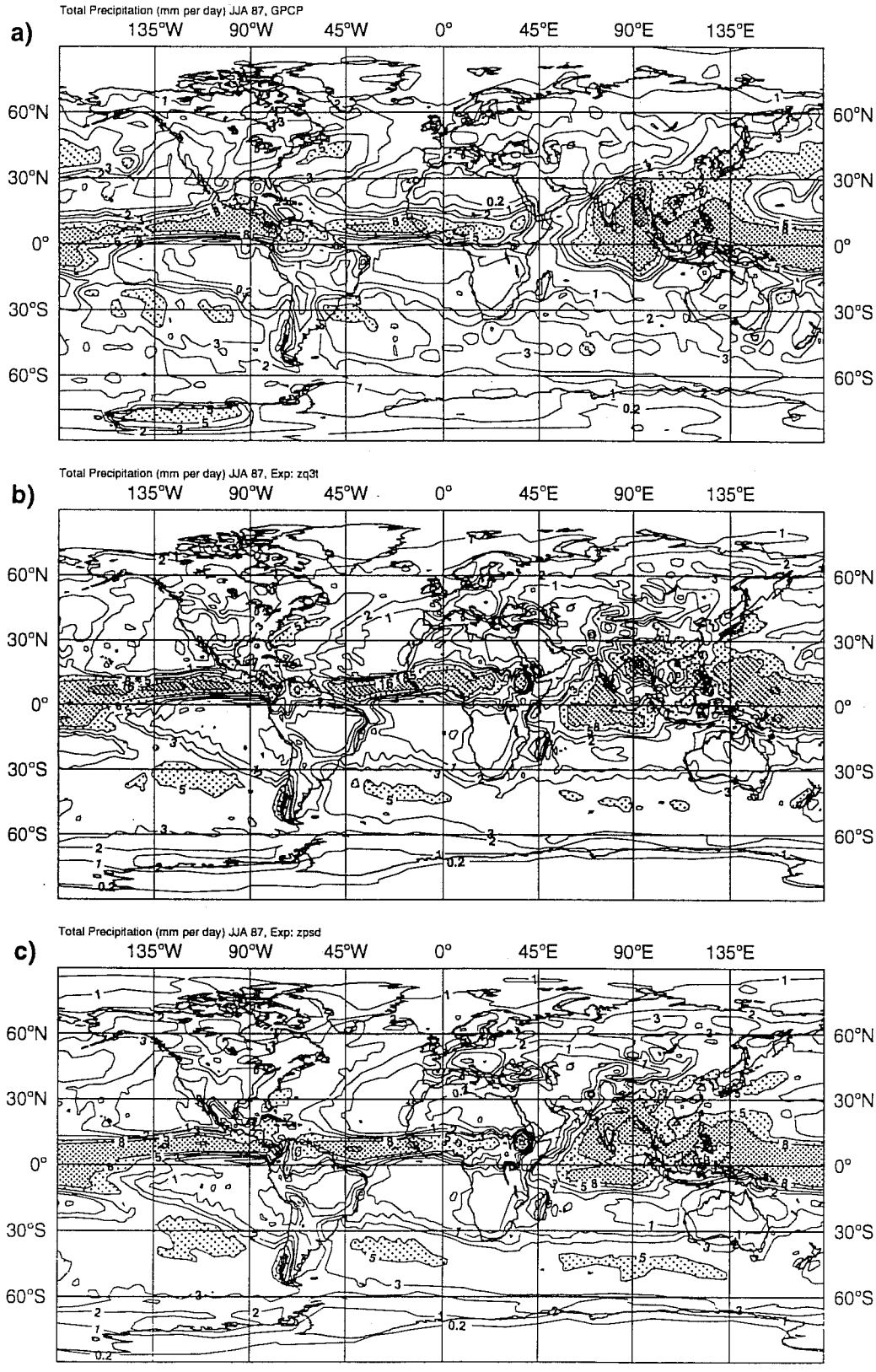

Fig. 2 Total precipitation (mm/day) for June/July/August 1987 from (a) GPCP climatology and from 125 day T63L31 simulations using CY16R2 plus correction to convective momentum transport formulation): (b) control simulation and (c) simulation with PACKAGE F. Model results are an average over an ensemble of three simulations (see text for details). Contours at 0.1,1,2,3,5,8,16 and 32 mm/day, shaded above 5mm/day.

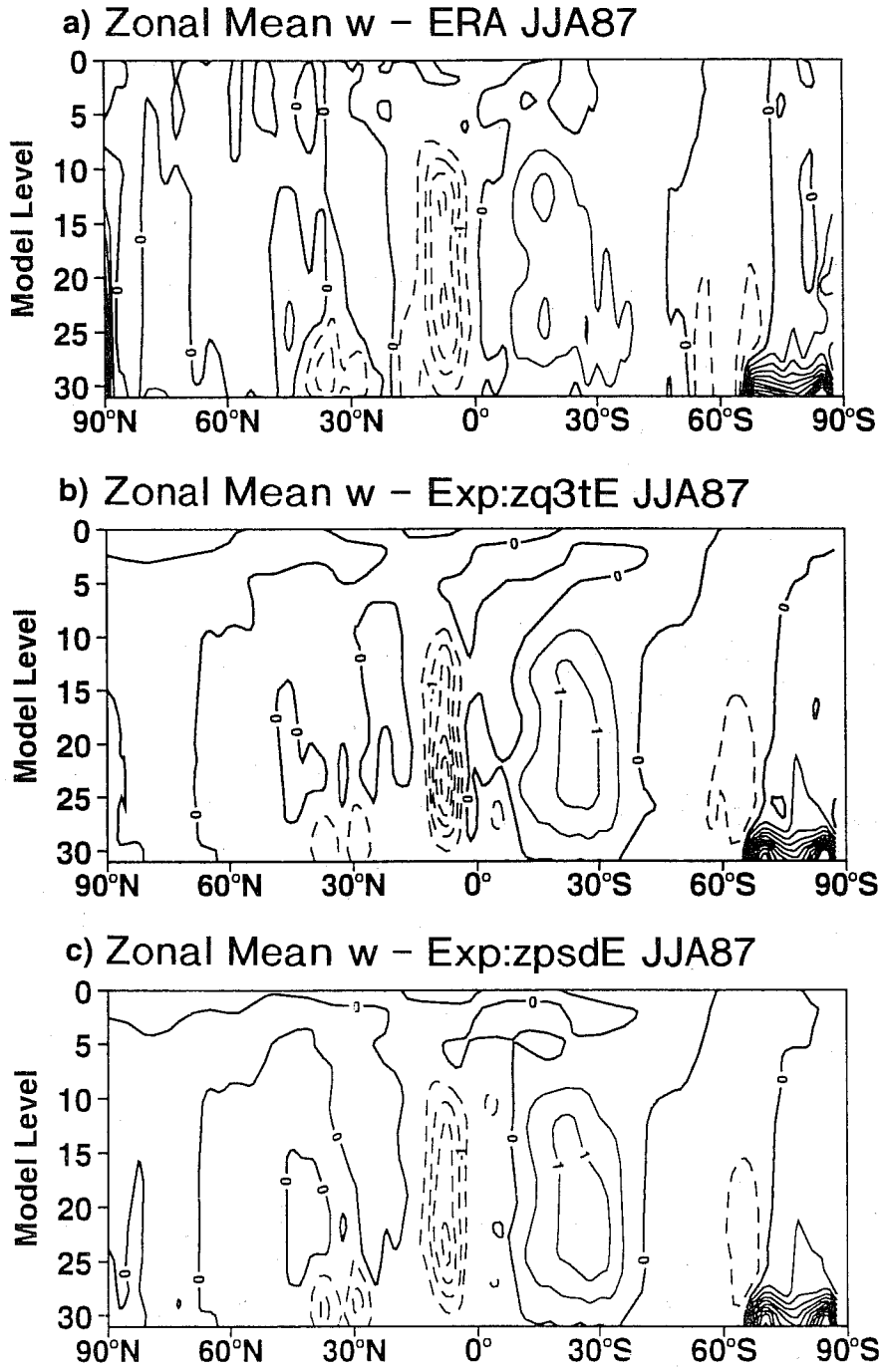

Fig. 3 Zonal mean omega (hPa/hr) for June/July/August 1987 from (a) ERA and from 125 day T63L31 simulations (using CY16R2 plus correction to convective momentum transport formulation): (b) control simulation and (c) simulation with PACKAGE F. Model results are an average over an ensemble of three simulations (see text for details). Contour interval: 0.5hPa/hr.

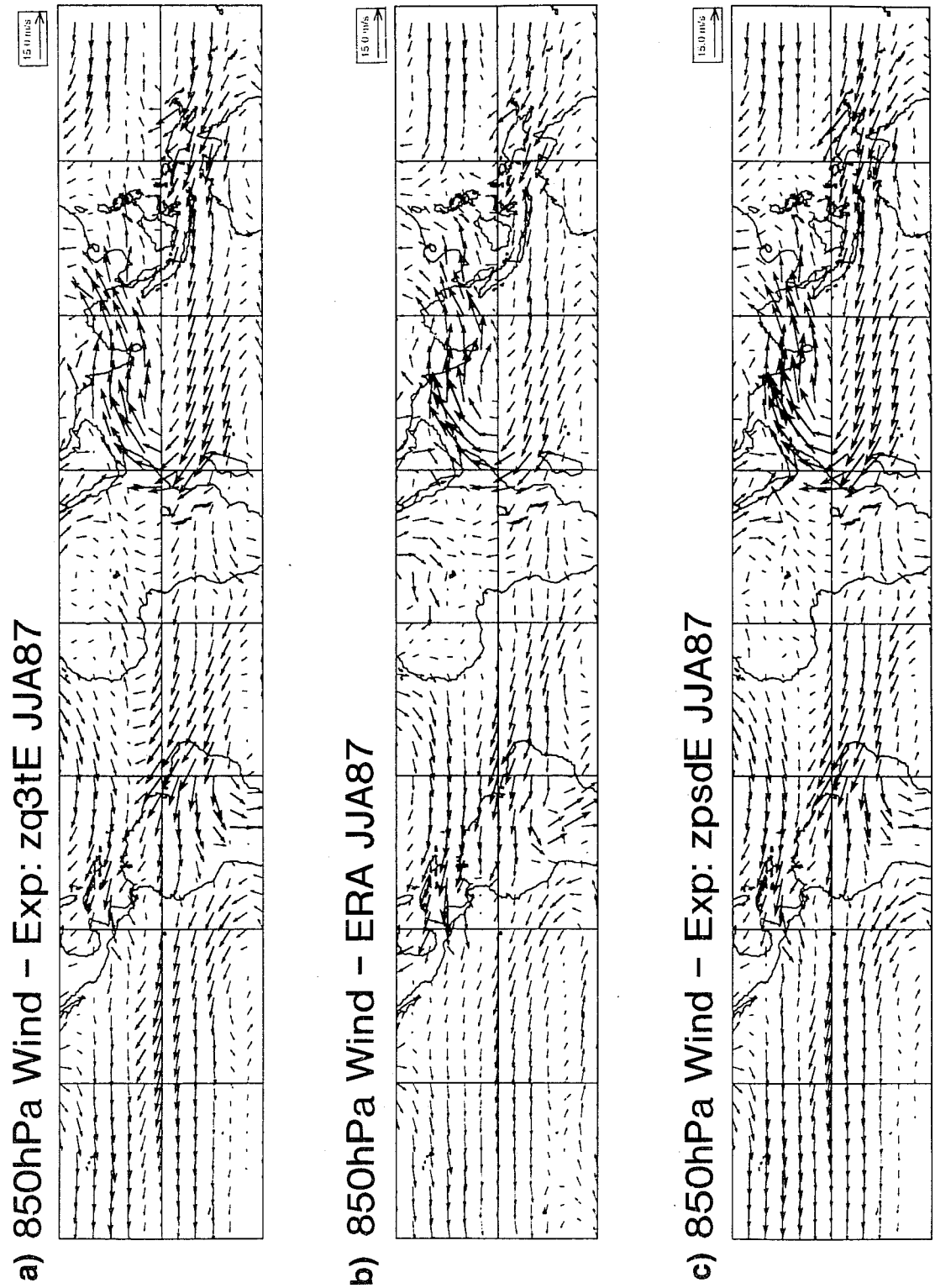

Fig. 4 850hPa wind from the tropical belt for June/July/August 1987 from (b) ERA and from 125 day T63L31 simulations (using CY16R2 plus correction to convective momentum transport formulation): (a) control simulation and (c) simulation with PACKAGE F. Model results are an average over an ensemble of three simulations (see text for details).

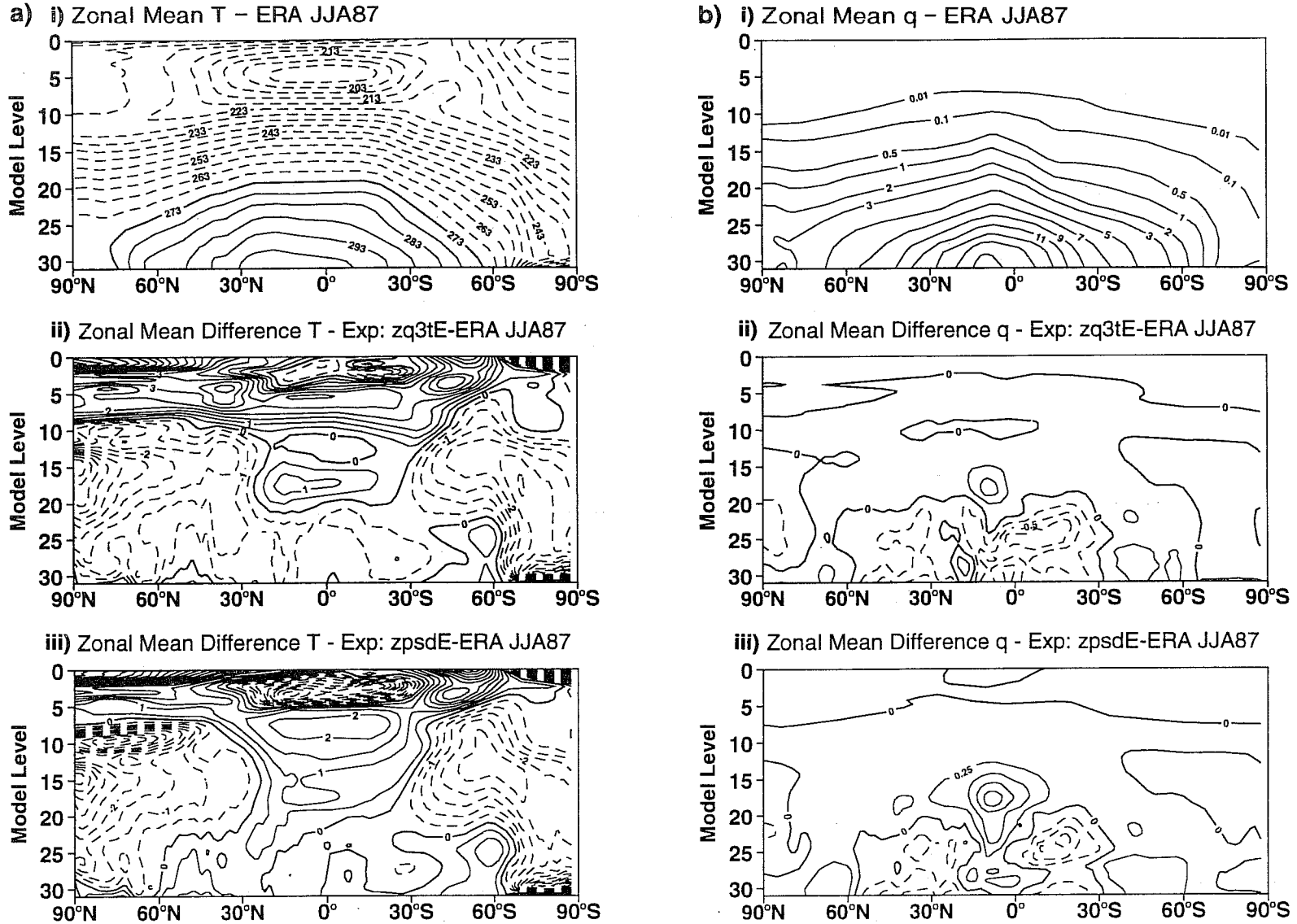

Fig. 5 a) (i) Zonal mean temperature (K) from ERA for June/July/August 1987 together with differences from ERA of 125 day T63L31 simulations (using CY16R2 plus correction to convective momentum transport formulation): (ii) control simulation and (iii) simulation with PACKAGE F. Model results are an average over an ensemble of three simulations (see text for details). Contour interval: 0.5K. 5b) (i) Zonal mean mixing ratio (g/kg) from ERA for June/July/August 1987 together with differences from ERA of 125 day T63L31 simulations (using CY16R2 plus correction to convective momentum transport formulation): (ii) control simulation and (iii) simulation with PACKAGE F. Model results are an average over an ensemble of three simulations (see text for details). Contour interval: 0.25g/kg.

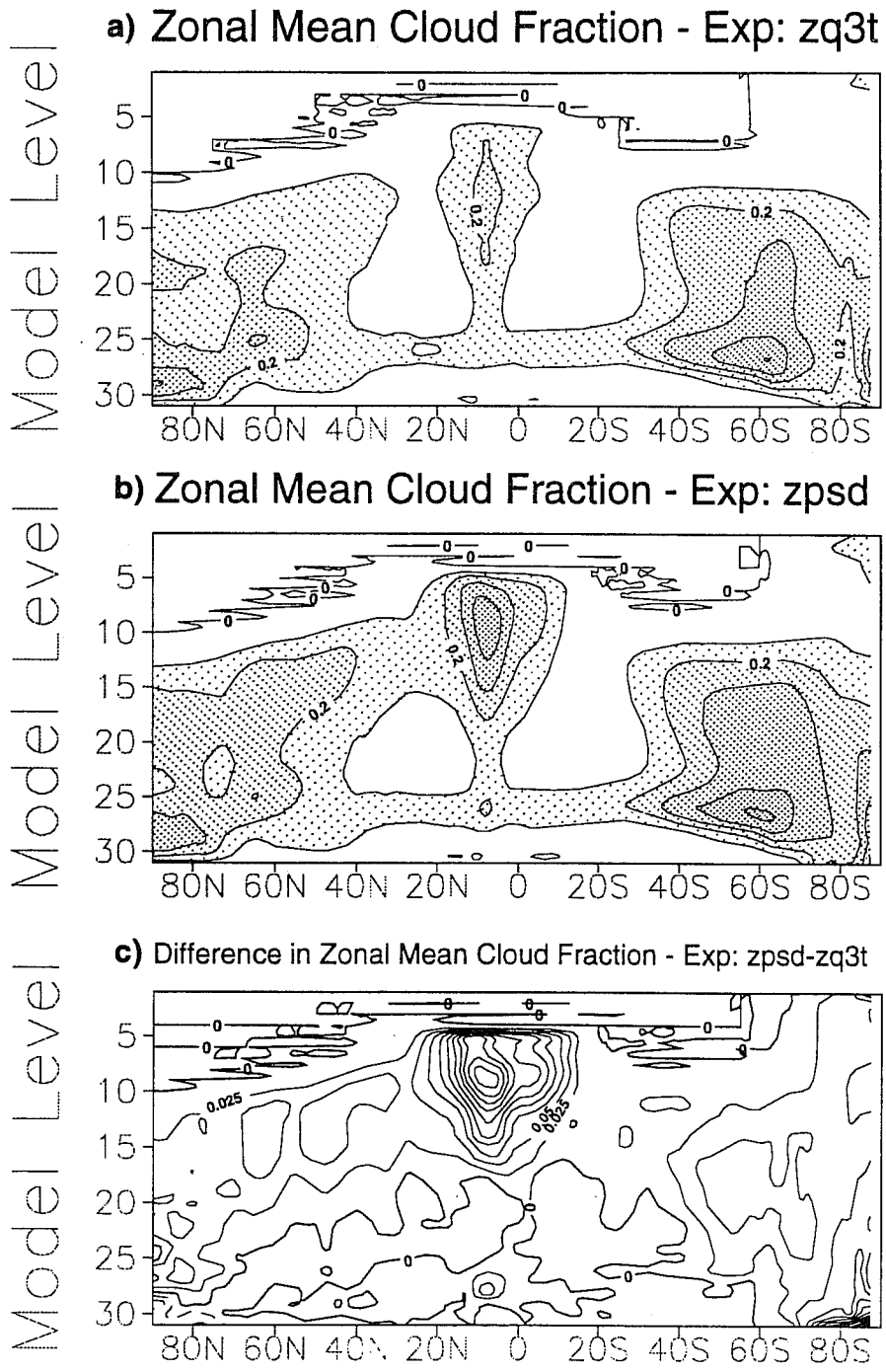

Fig. 6 Zonal mean cloud fraction for June/July/August 1987 from 125 day T63L31 simulations (using CY16R2 plus correction to convective momentum transport formulation): (a) control simulation and (b) simulation with PACKAGE F and (c) PACKAGE F - control. Model results are an average over an ensemble of three simulations (see text for details). Contour interval: 0.1 on plots of cloud fraction, 0.025 on plot of differences.

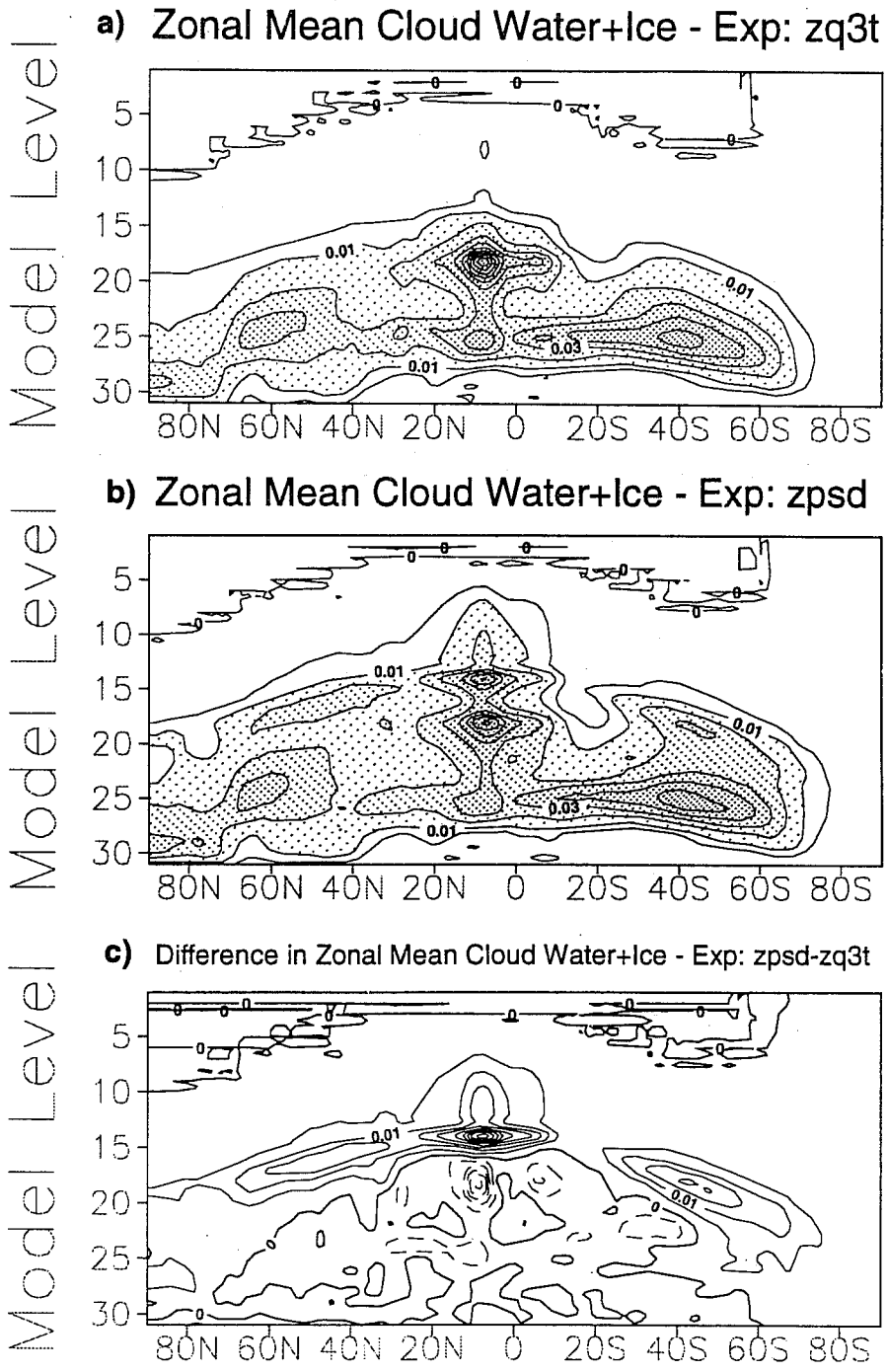

Fig. 7 Zonal mean cloud water plus ice content (g/kg) for June/July/August 1987 from 125 day T63L31 simulations (using CY16R2 plus correction to convective momentum transport formulation): (a) control simulation, (b) simulation with PACKAGE F and (c) PACKAGE F - control. Model results are an average over an ensemble of three simulations (see text for details). On plots of cloud water, contours at 0.001, 0.01,0.1,0.2,0.3,0.4,0.5 g/kg. On plots of difference in cloud water the contour interval is 0.005g/kg.

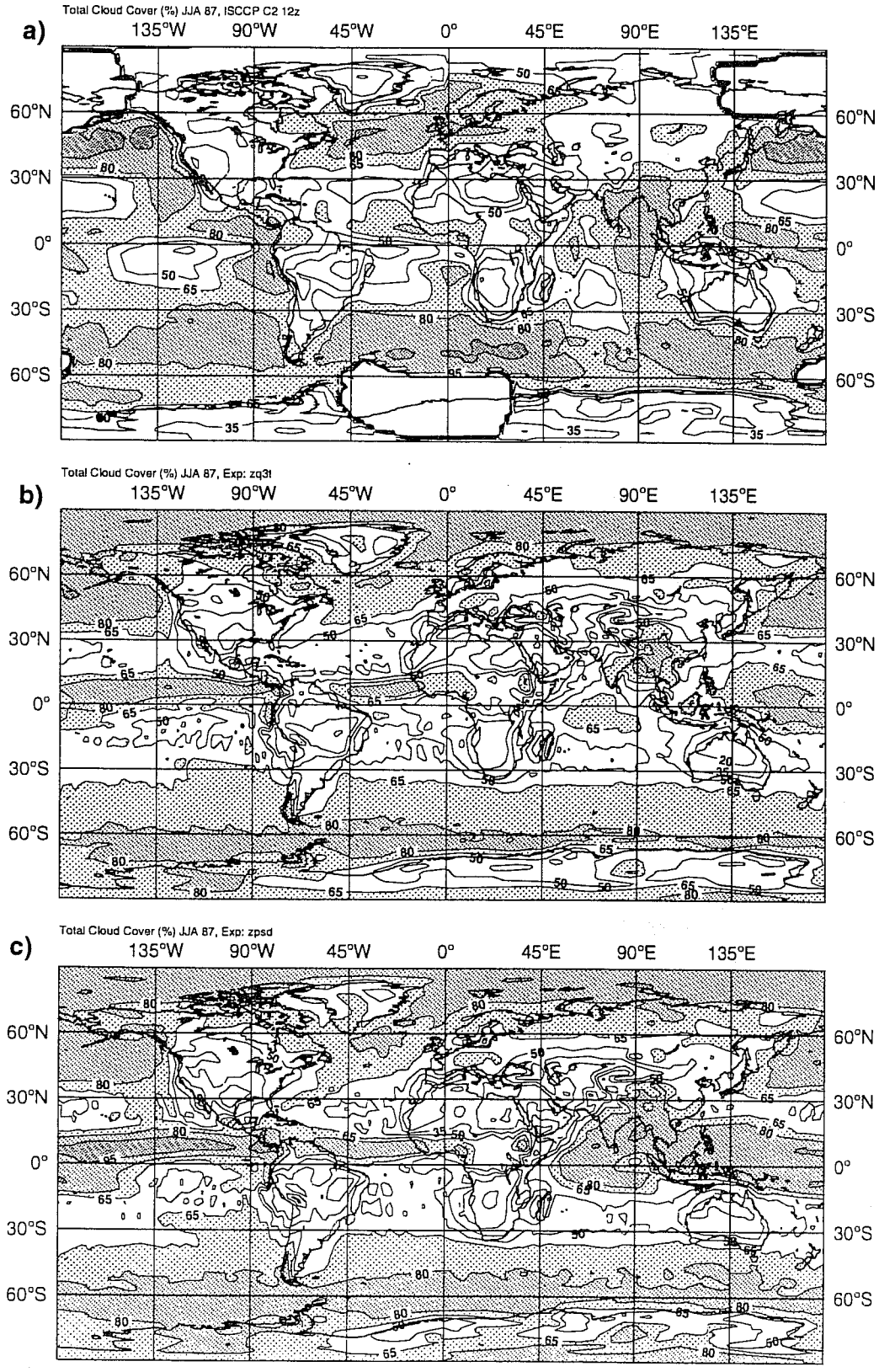

Fig. 8 Total cloud cover (%) for June/July/August 1987 from (a) ISCCP and from 125 day T63L31 simulations (using CY16R2 plus correction to convective momentum transport formulation): (b) control simulation and (c) simulation with PACKAGE F. Model results are an average over an ensemble of three simulations (see text for details). Contours at 5,20,35,50,65,80 and 95%. Shaded above 65%.

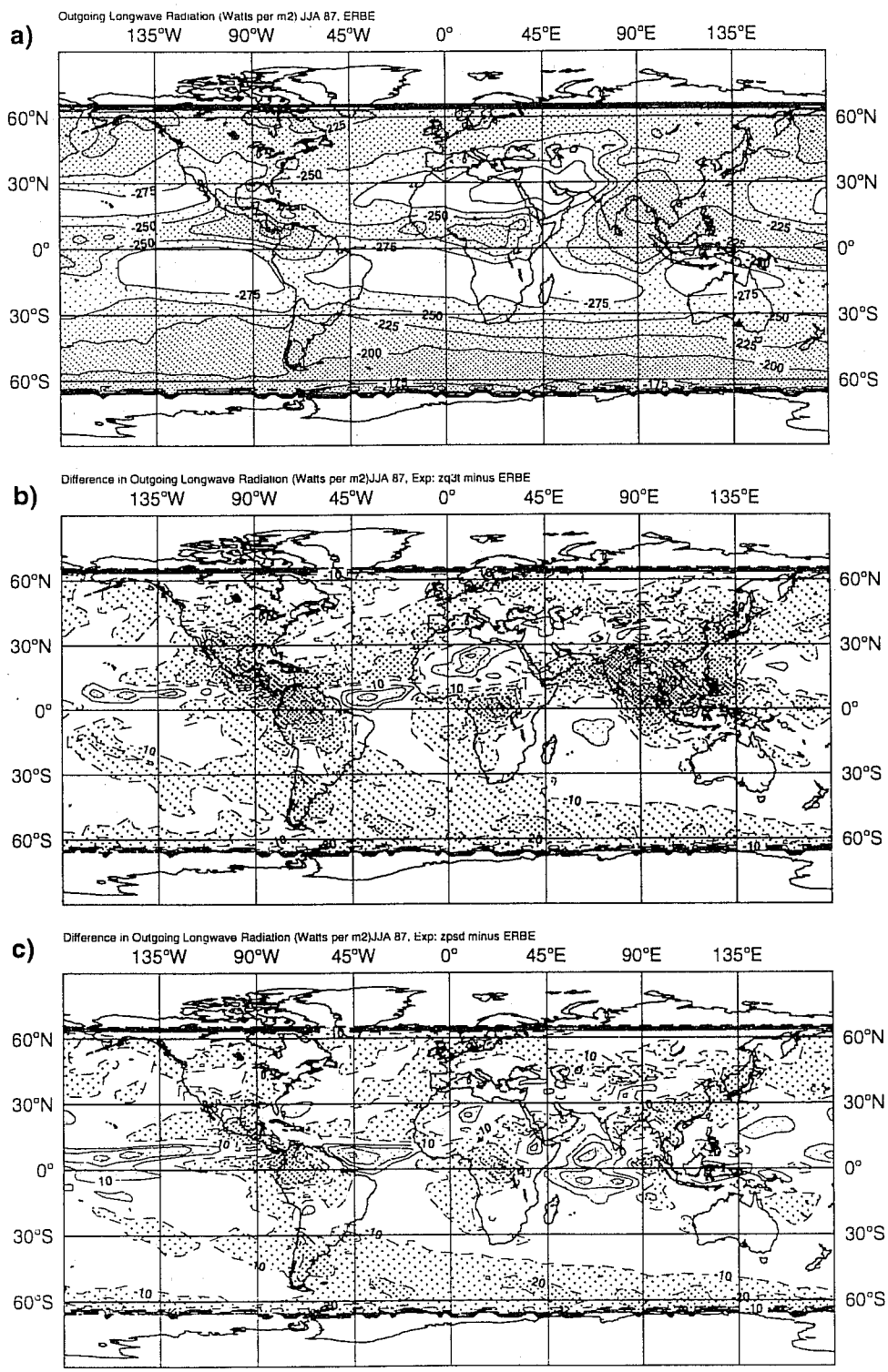

Fig. 9 Outgoing Longwave Radiation (OLR - Wm^{-2}) for June/July/August 1987 from (a) ERBE and difference of OLR from 125 day T63L31 simulations (using CY16R2 plus correction to convective momentum transport formulation) from ERBE: (b) control simulation and (c) simulation with PACKAGE F. Model results are an average over an ensemble of three simulations (see text for details). On OLR plot, contour interval is $25Wm^{-2}$, shaded below $275Wm^{-2}$. On plots of differences, contour interval is $10Wm^{-2}$, positive values: solid contour, light shading above $10Wm^{-2}$, negative values: dashed contour, dark shading below $-10Wm^{-2}$.

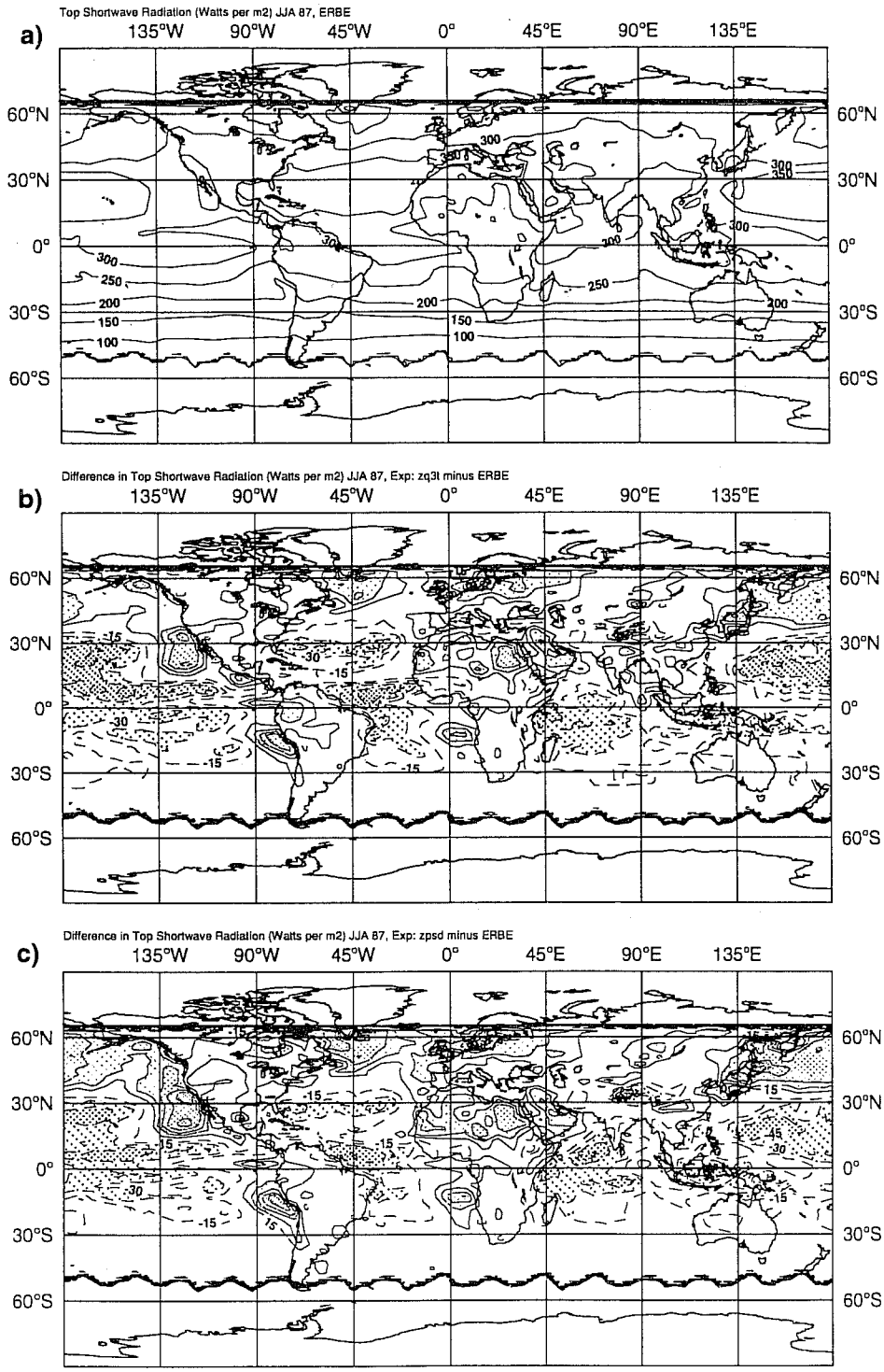

Fig. 10 Top of atmosphere shortwave radiation (TOA SW - Wm^{-2}) for June/July/August 1987 from (a) ERBE and difference of TOA SW from 125 day T63L31 simulations (using CY16R2 plus correction to convective momentum transport formulation) from ERBE: (b) control simulation and (c) simulation with PACKAGE F. Model results are an average over an ensemble of three simulations (see text for details). On plot of TOA SW radiation contour interval is $50Wm^{-2}$. On difference plots, contour interval is $15Wm^{-2}$, positive values: solid contour, light shading above $30Wm^{-2}$, negative values: dashed contour, dark shading below $-30Wm^{-2}$.

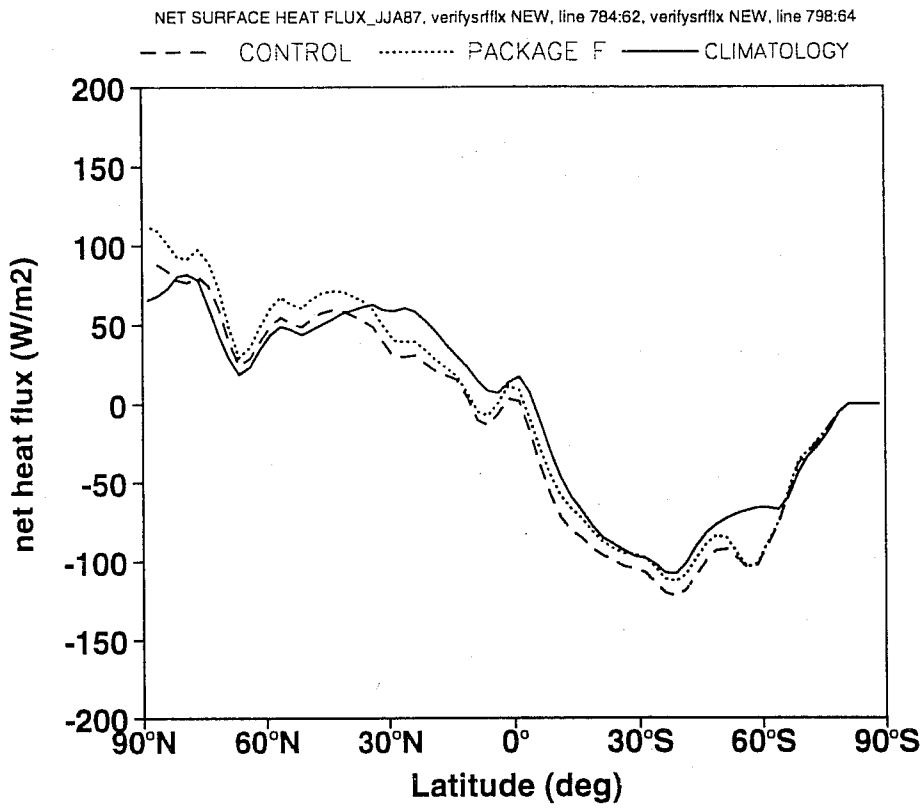

Fig. 11 Zonal mean ocean surface net heat flux for June/July/August 1987 from 125 day T63L31 simulations (using CY16R2 plus correction to convective momentum transport formulation); climatology of da Silva: solid line, simulation with PACKAGE F: dotted line and control simulation: dashed line. Model results are an average over an ensemble of three simulations (see text for details).

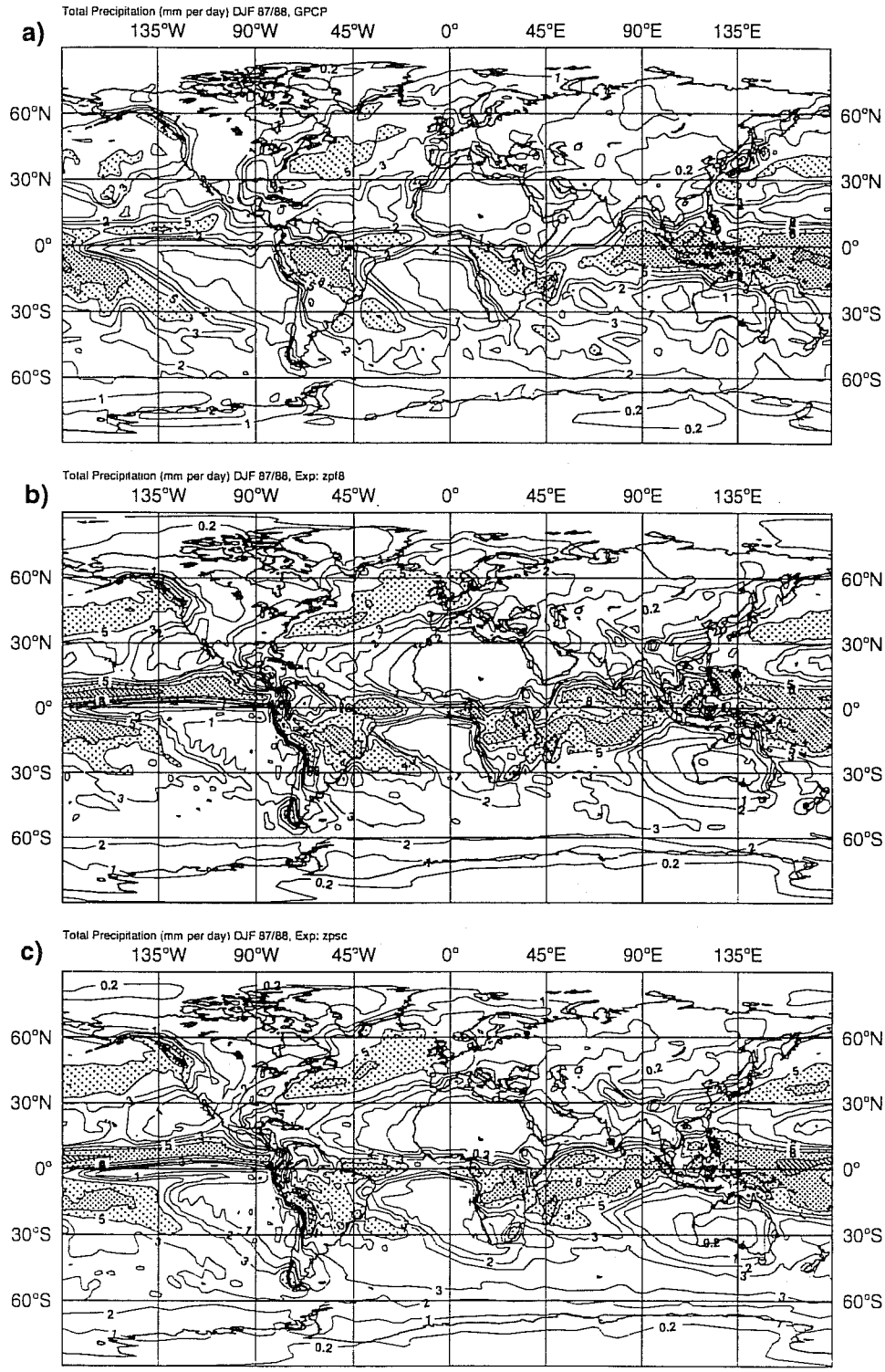

Fig. 12 Total precipitation (mm/day) for December/January/February 1987/88 from (a) GPCP climatology, from 125 day T63L31 simulations (using CY16R2 plus correction to convective momentum transport formulation): (b) control simulation and (c) simulation with PACKAGE F. Model results are an average over an ensemble of three simulations (see text for details). Contours at 0.1,1,2,3,5,8,16 and 32 mm/day, shaded above 5mm/day.

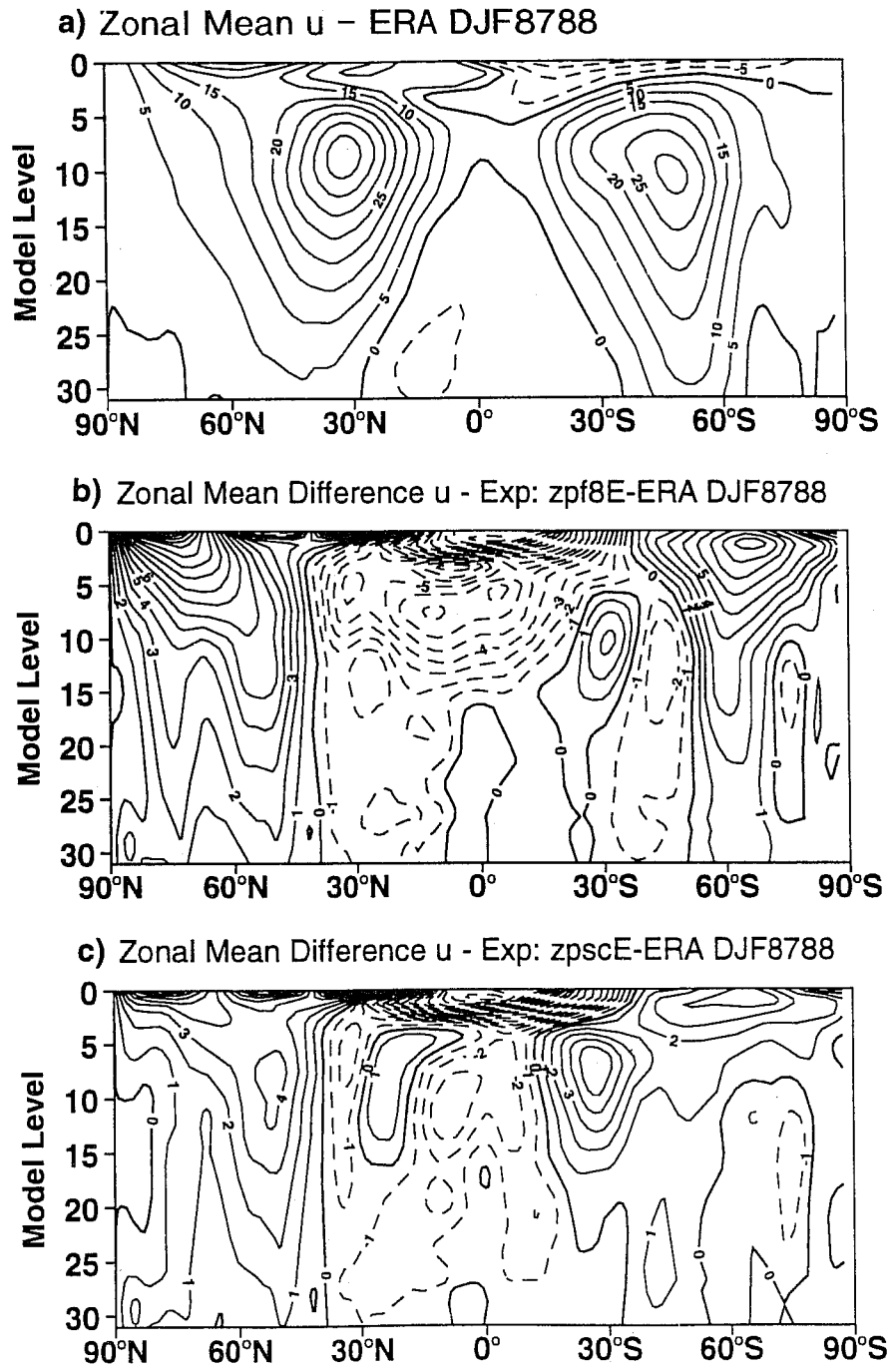

Fig. 13 Zonal mean wind (ms^{-1}) from (a) ERA for December/January/February 1987/88 and wind error (compared to ERA data) for same period from 125 day T63L31 simulations (using CY16R2 plus correction to convective momentum transport formulation); (b) control simulation and (c) simulation with PACKAGE F. Model results are an average over an ensemble of three simulations (see text for details). Contour interval: $1ms^{-1}$.

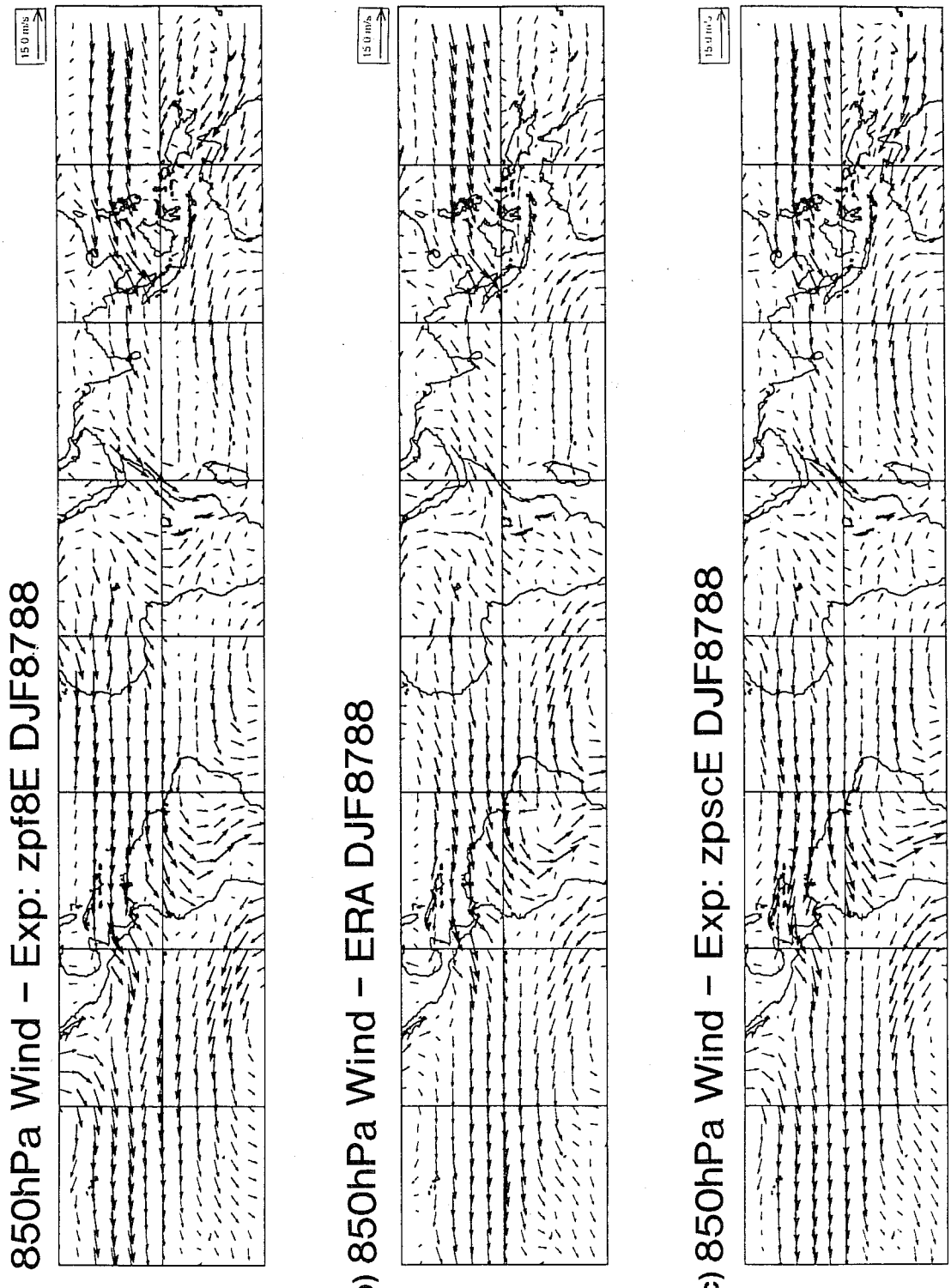

Fig. 14 850hPa wind from the tropical belt for December/January/February 1987/88 from (b) ERA and from 125 day T63L31 simulations (using CY16R2 plus correction to convective momentum transport formulation): (a) control simulation and (c) simulation with PACKAGE F. Model results are an average over an ensemble of three simulations (see text for details).

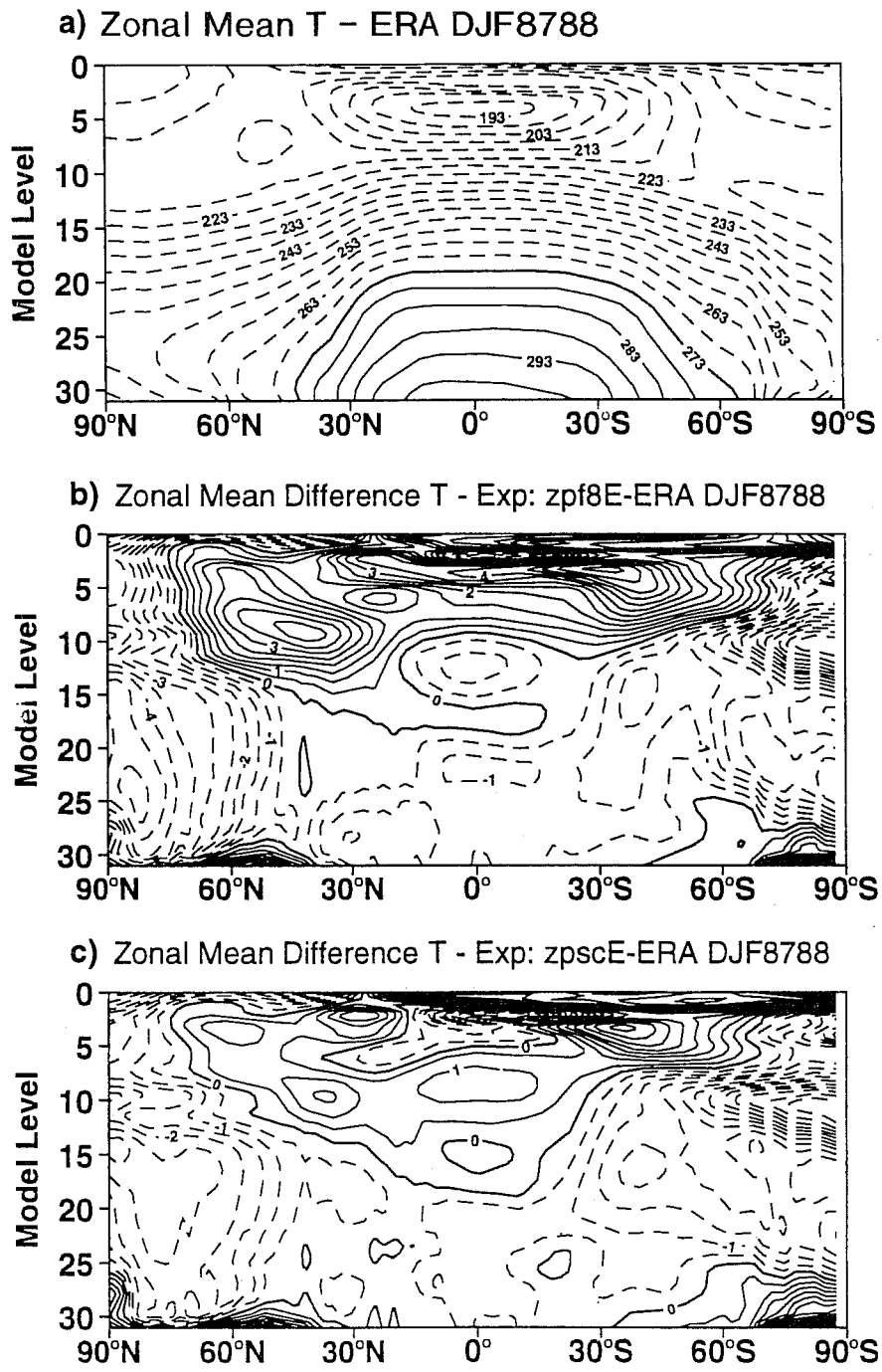

Fig. 15 (a) Zonal mean temperature (K) from ERA for December/January/February 1987/88 together with differences from ERA of 125 day T63L31 simulations (using CY16R2 plus correction to convective momentum transport formulation): (b) control simulation and (c) simulation with PACKAGE F. Model results are an average over an ensemble of three simulations (see text for details). Contour interval: 0.5K.

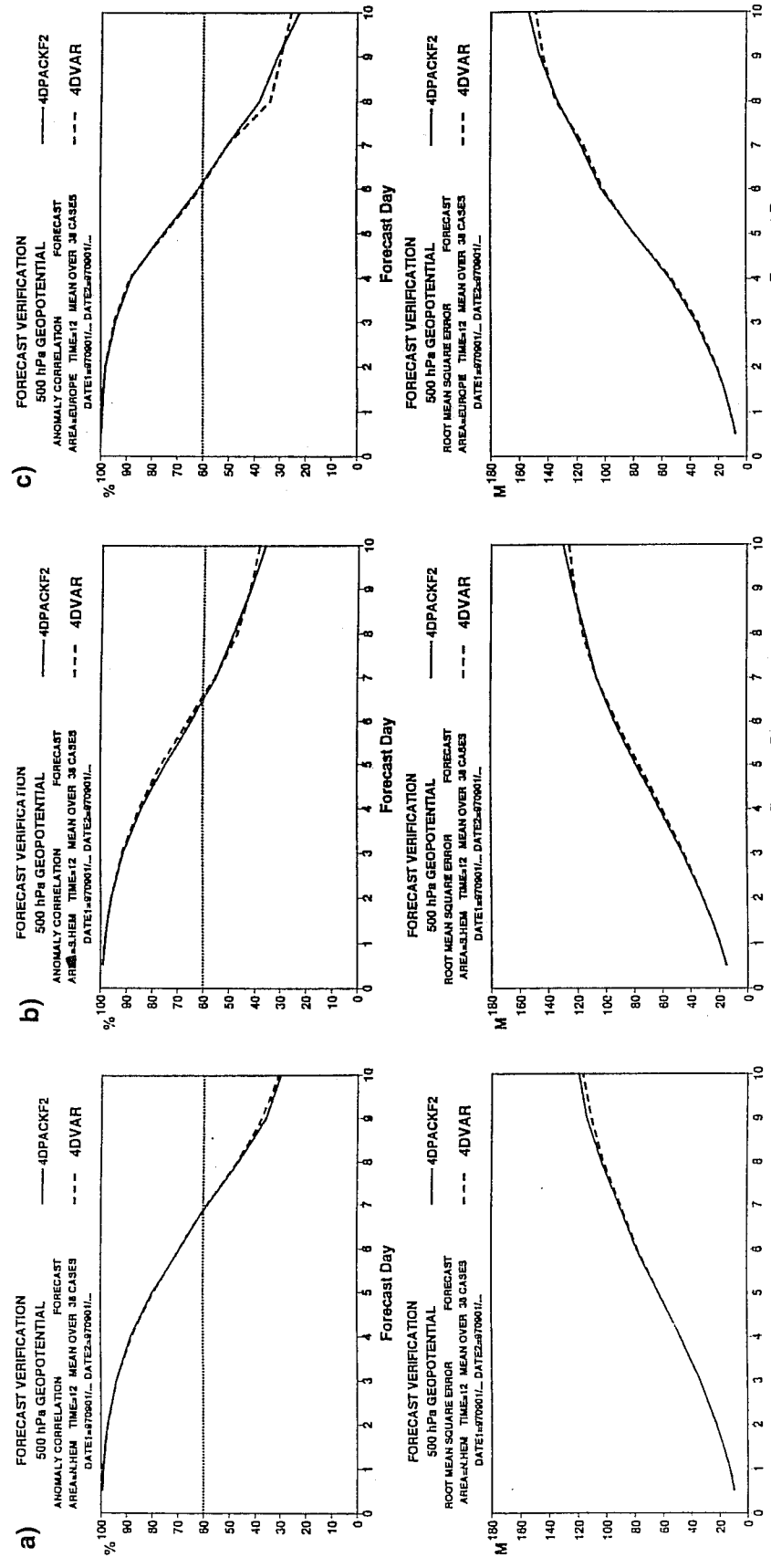

Fig. 16 Mean (38 cases) 500hPa anomaly correlation and root mean square error scores from 4D-Var experiments for January and September 1997 periods; PACKAGE F - solid line, control - dashed line. (a) northern hemisphere, (b) southern hemisphere and (c) Europe

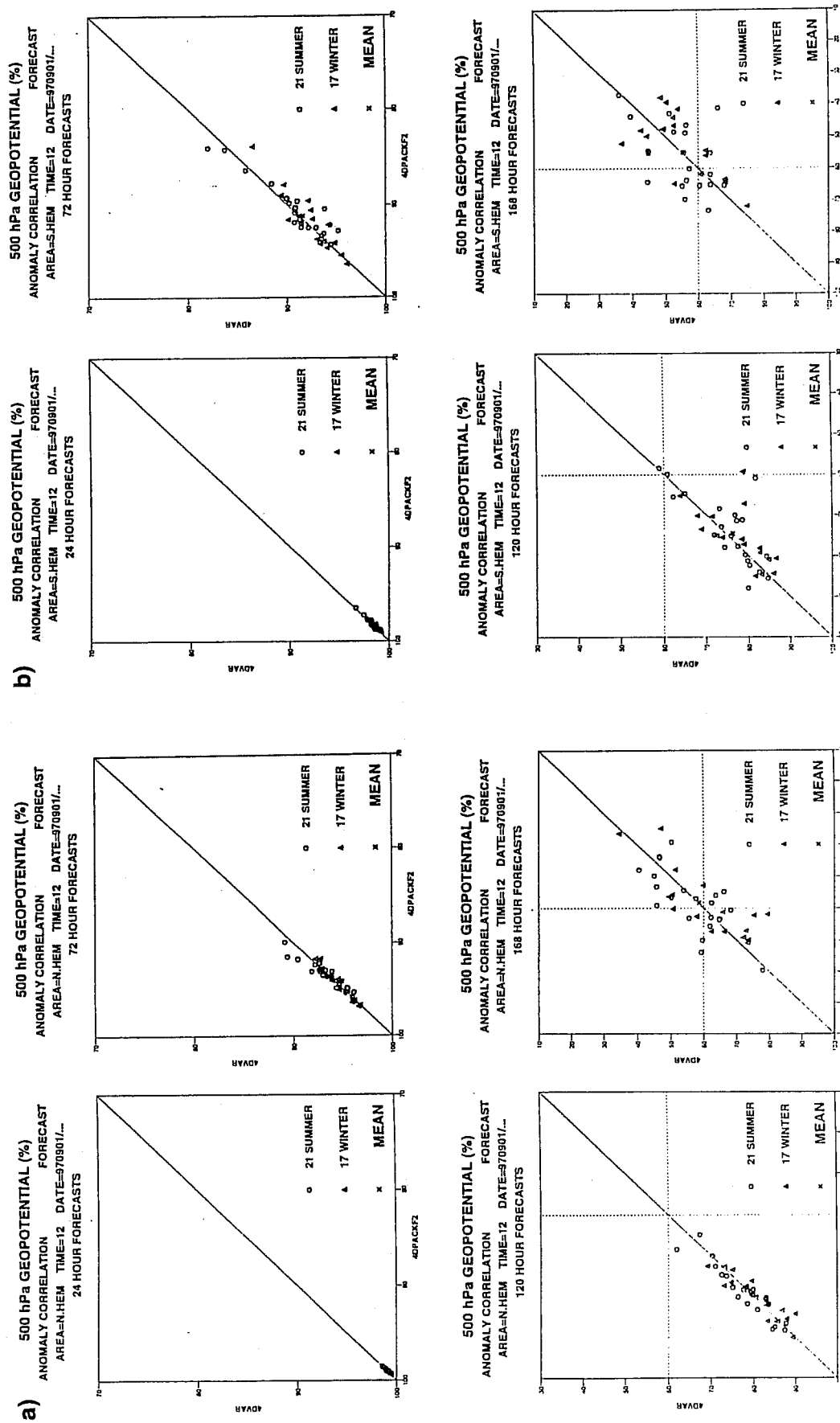

Fig. 17 Scatter plots for 500hPa anomaly correlation from 4D-Var experimentation for 38 forecasts for January and September 1997 periods. Axes labels; PACKAGE F - 4DPACKF2; control - 4DVAR. (a) northern hemisphere, (b) southern hemisphere and (c) Europe

c)

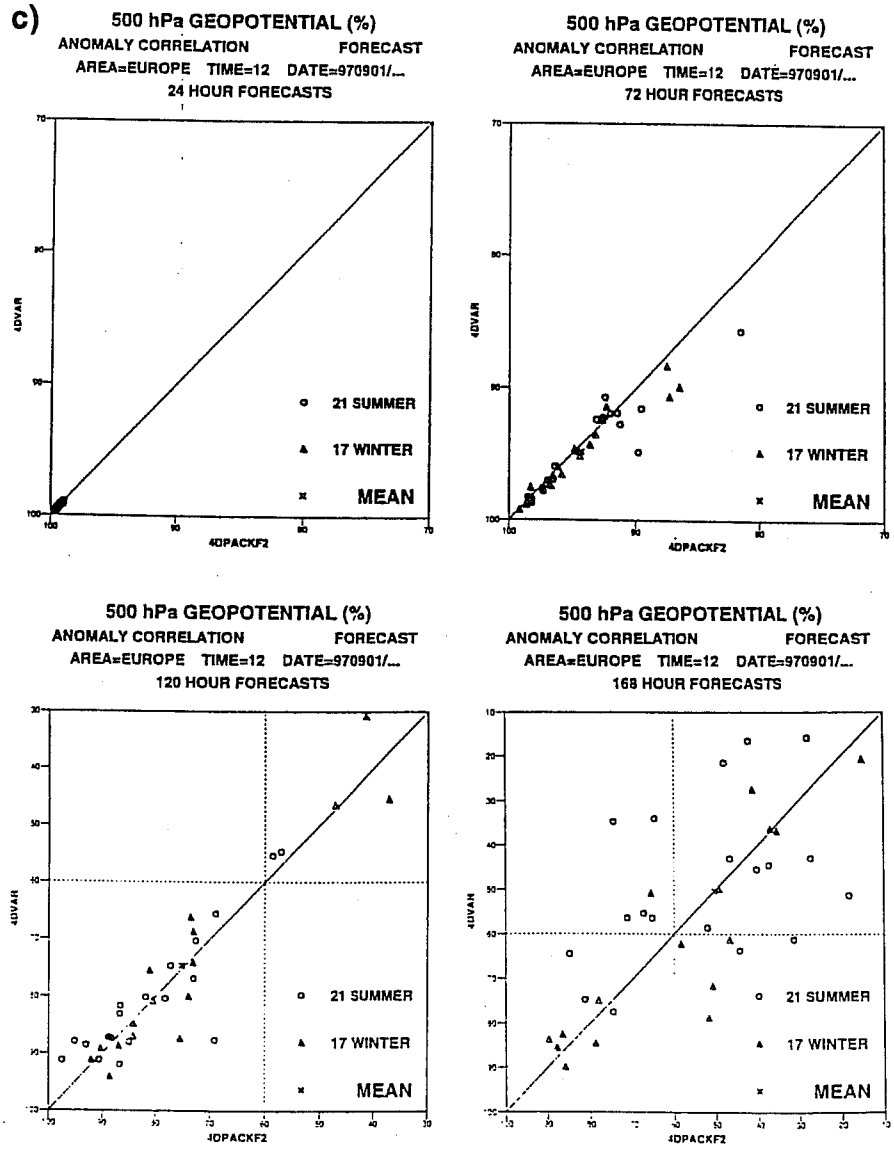

Fig. 17 continued

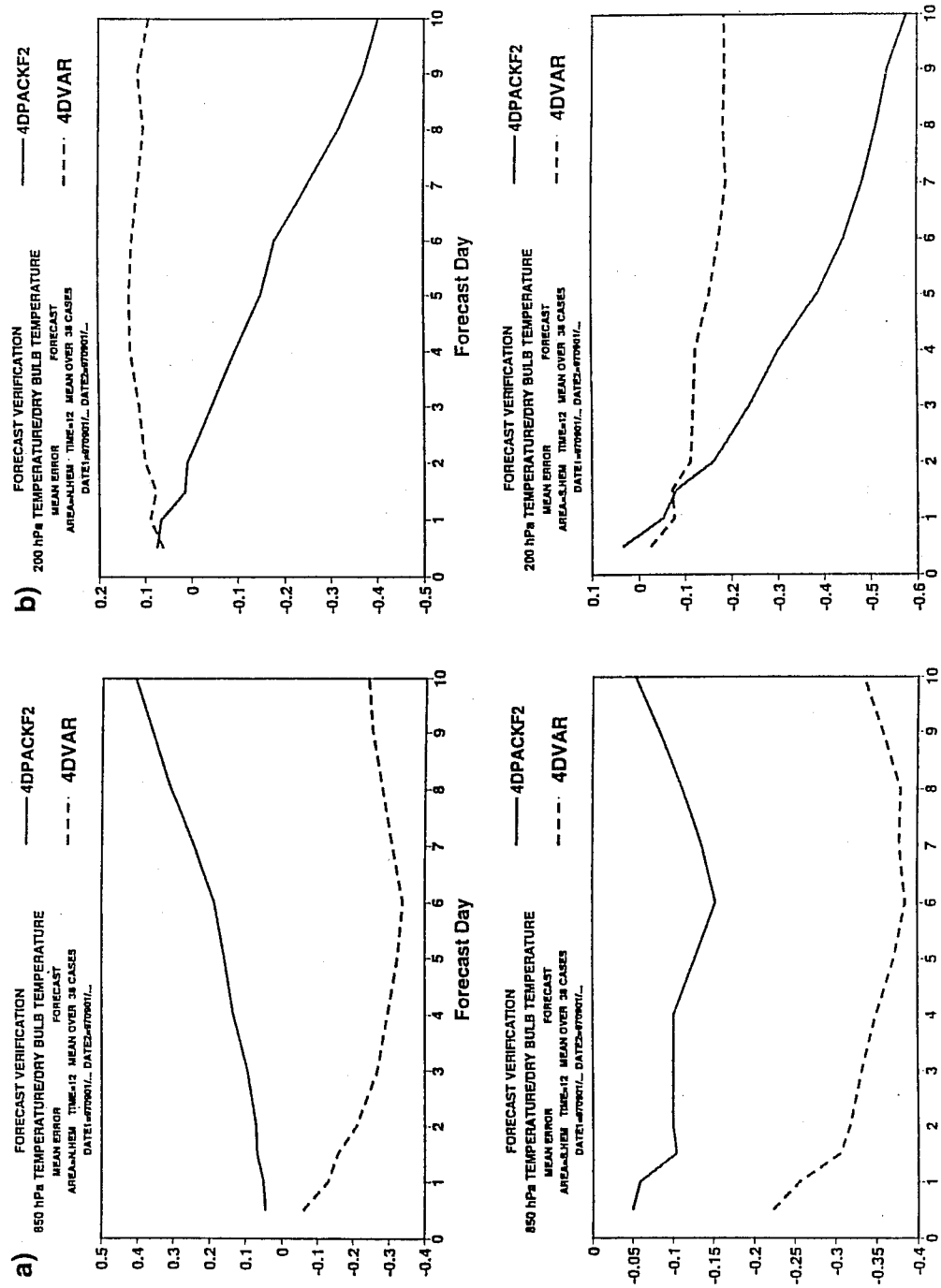

Fig. 18 Mean (38 cases) (a) 850hPa and (b) 200hPa temperature bias for northern (top panel) and southern (bottom panel) hemispheres from 4D-Var experiments for January and September 1997 periods; PACKAGE F - solid line; control - dashed line.

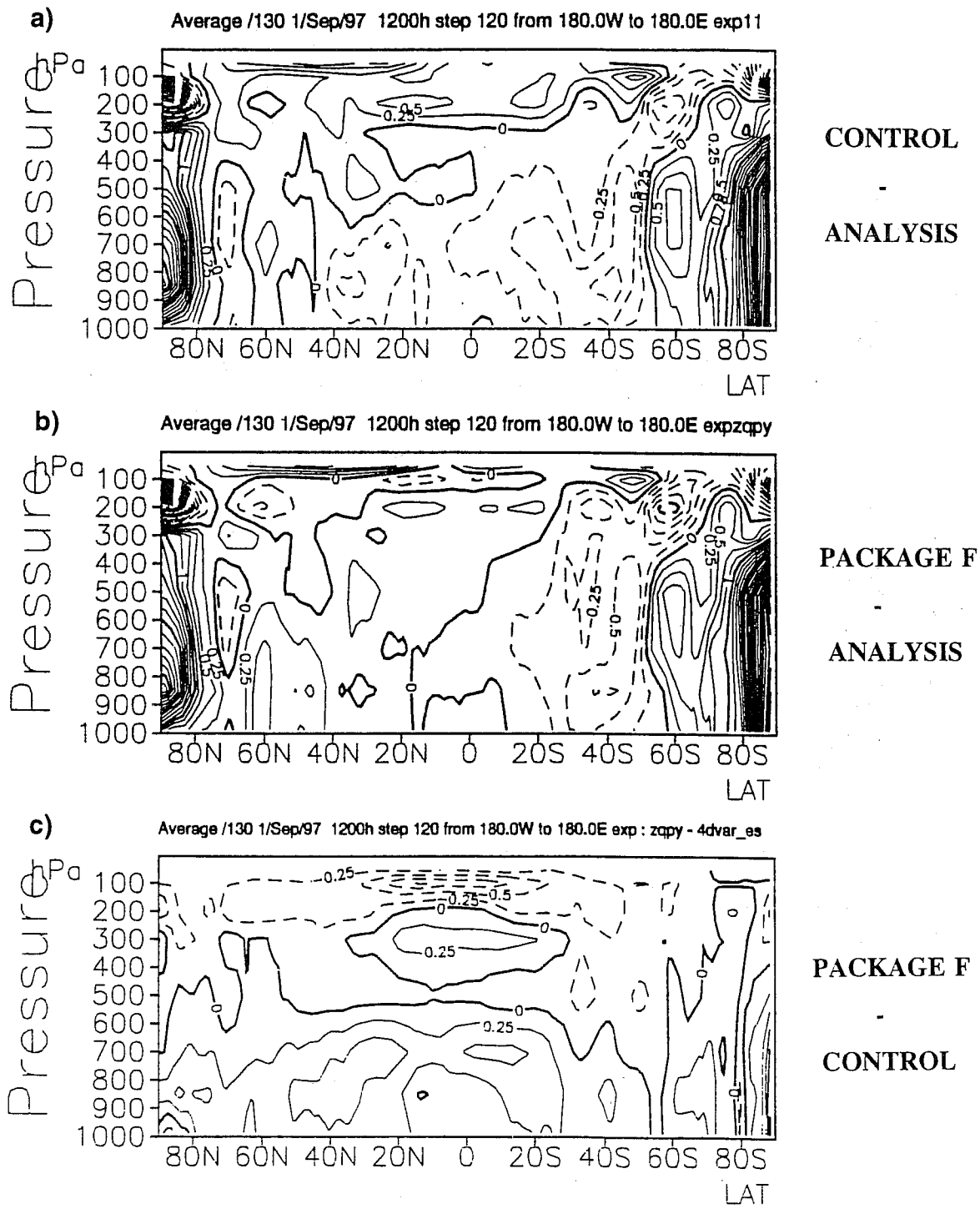

Fig. 19 Mean (15 cases) zonal mean day 5 temperature (K) bias (as measured against own analysis) from 4D-Var experimentation for September 1997 period (at CY16R4); (a) control forecasts, (b) PACKAGE F experiments and (c) difference between PACKAGE F and control simulation (bottom panel). Contour interval: 0.25K.

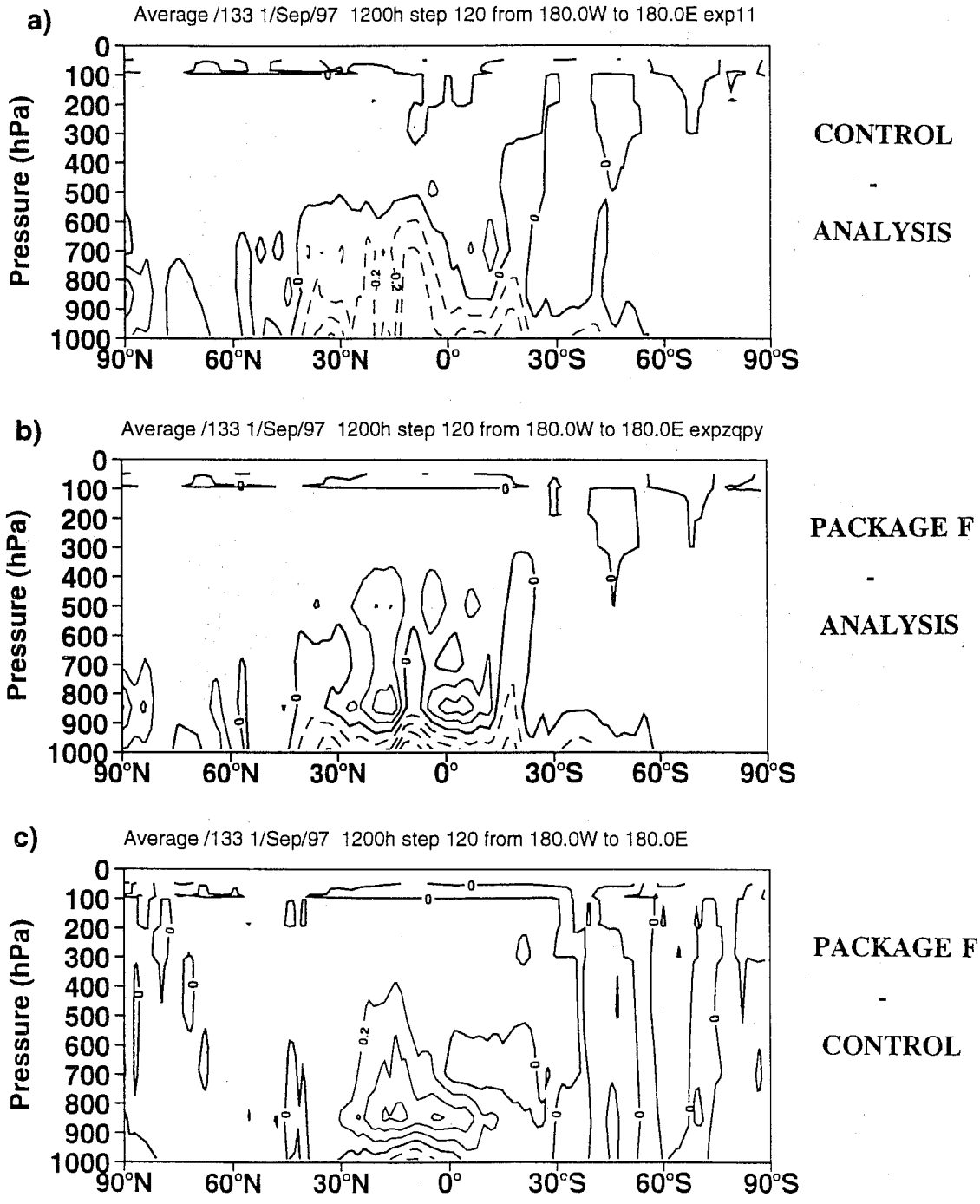

Fig. 20 Mean (15 cases) zonal mean day 5 mixing ratio (g/kg) bias (as measured against operational analysis) from 4D-Var experimentation for September 1997 period (at CY16R4); (a) control forecasts, (b) PACKAGE F experiments and (c) difference between PACKAGE F and control simulation (bottom panel). Contour interval: 0.25g/kg.

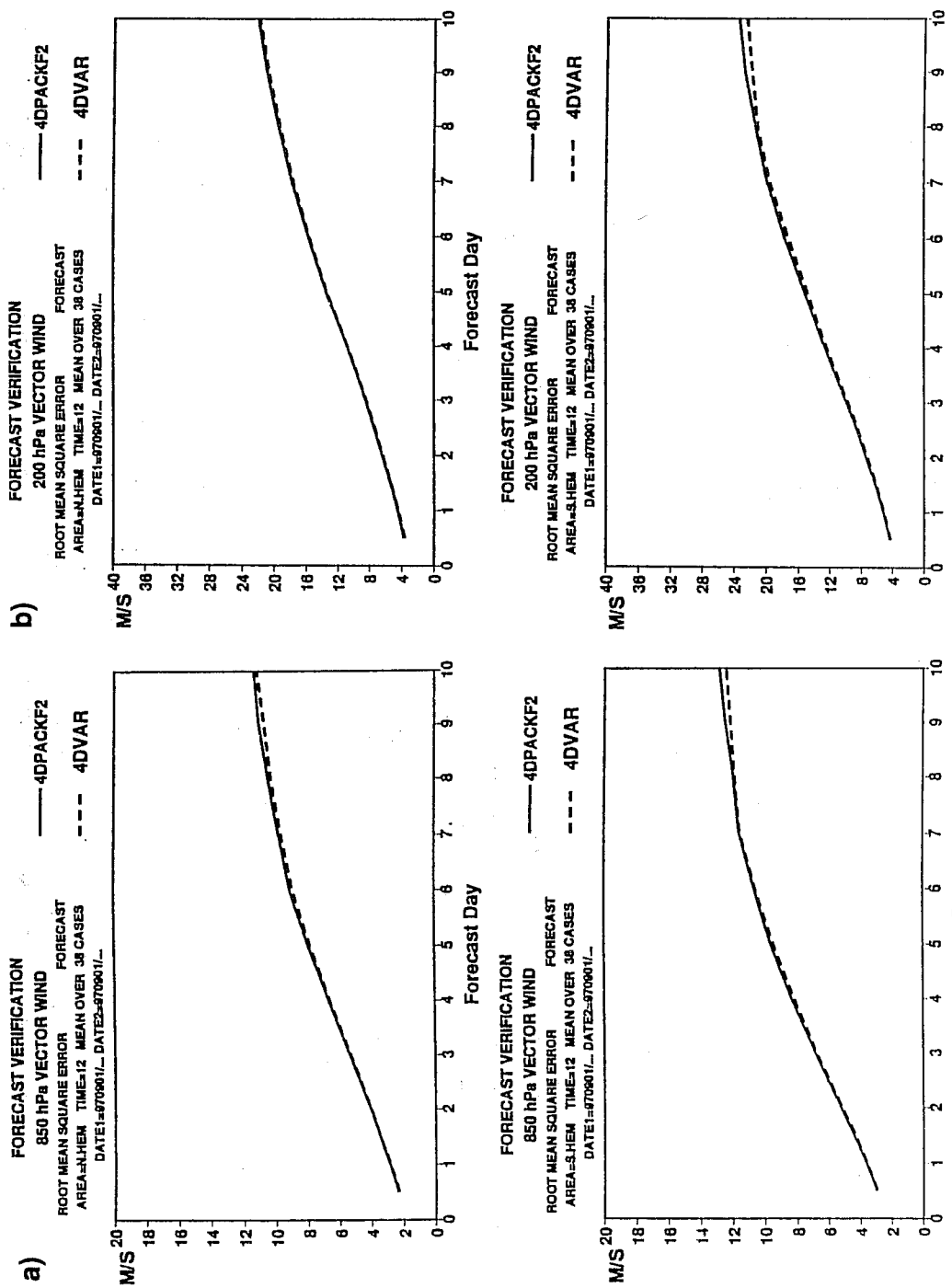

Fig. 21 Mean (38 cases) (a) 850hPa and (b) 200hPa root mean square wind errors for northern (top panel) and southern (bottom panel) hemispheres from 4D-Var experiments for January and September 1997 periods; PACKAGE F - solid line; control - dashed line.

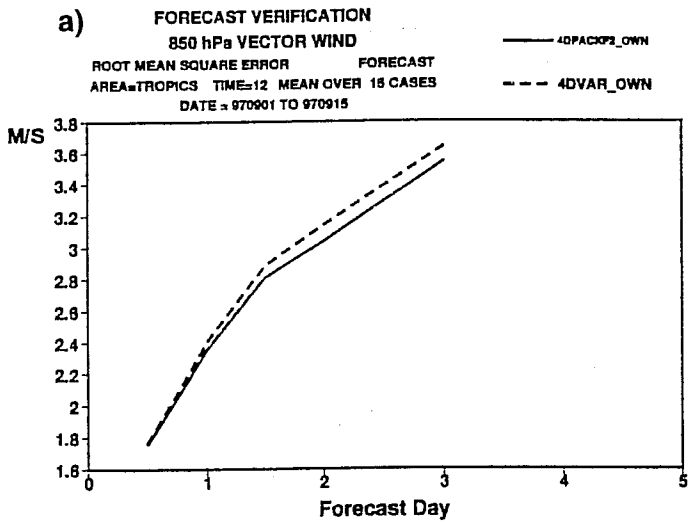

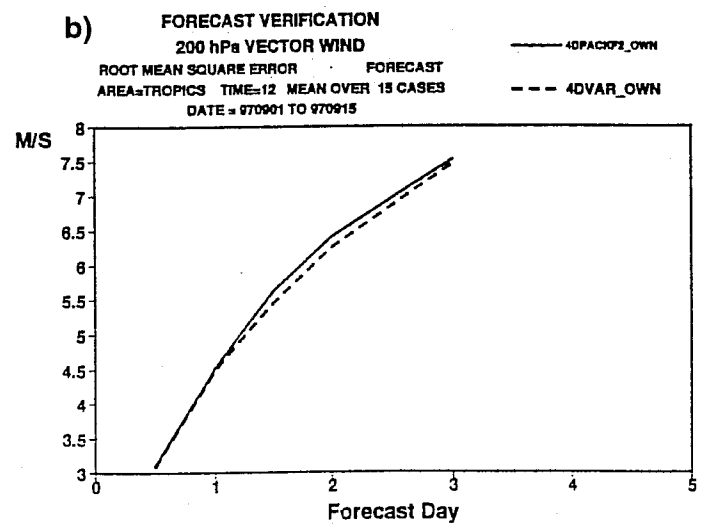

Fig. 22 Mean (15 cases) (a) 850hPa and (b) 200hPa root mean square wind errors for the tropics (measured against own analysis) from 4D-Var experiments for September 1997 period; PACKAGE F - solid line; control - dashed line.

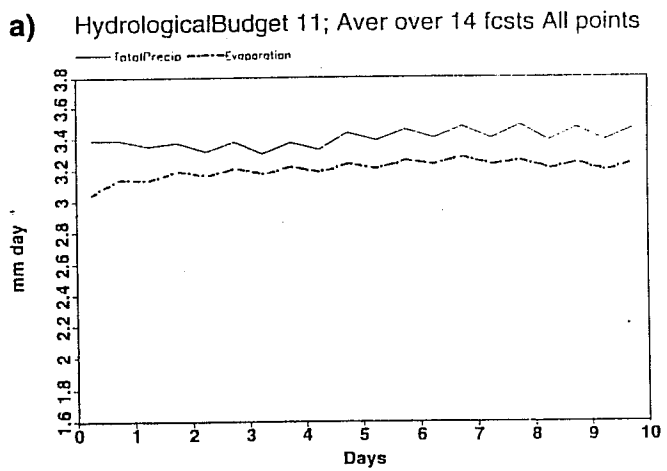

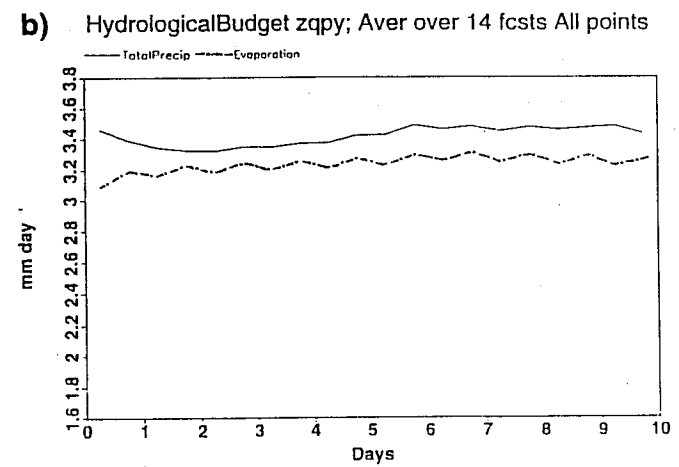

Fig. 23 Comparison of globally averaged total precipitation and surface evaporation through a 10 day forecast averaged over 14 cases from 4D-Var experimentation for September 1997 period. (a) Control forecasts; (b) PACKAGE F forecasts. Precipitation - solid line; evaporation - dashed line.

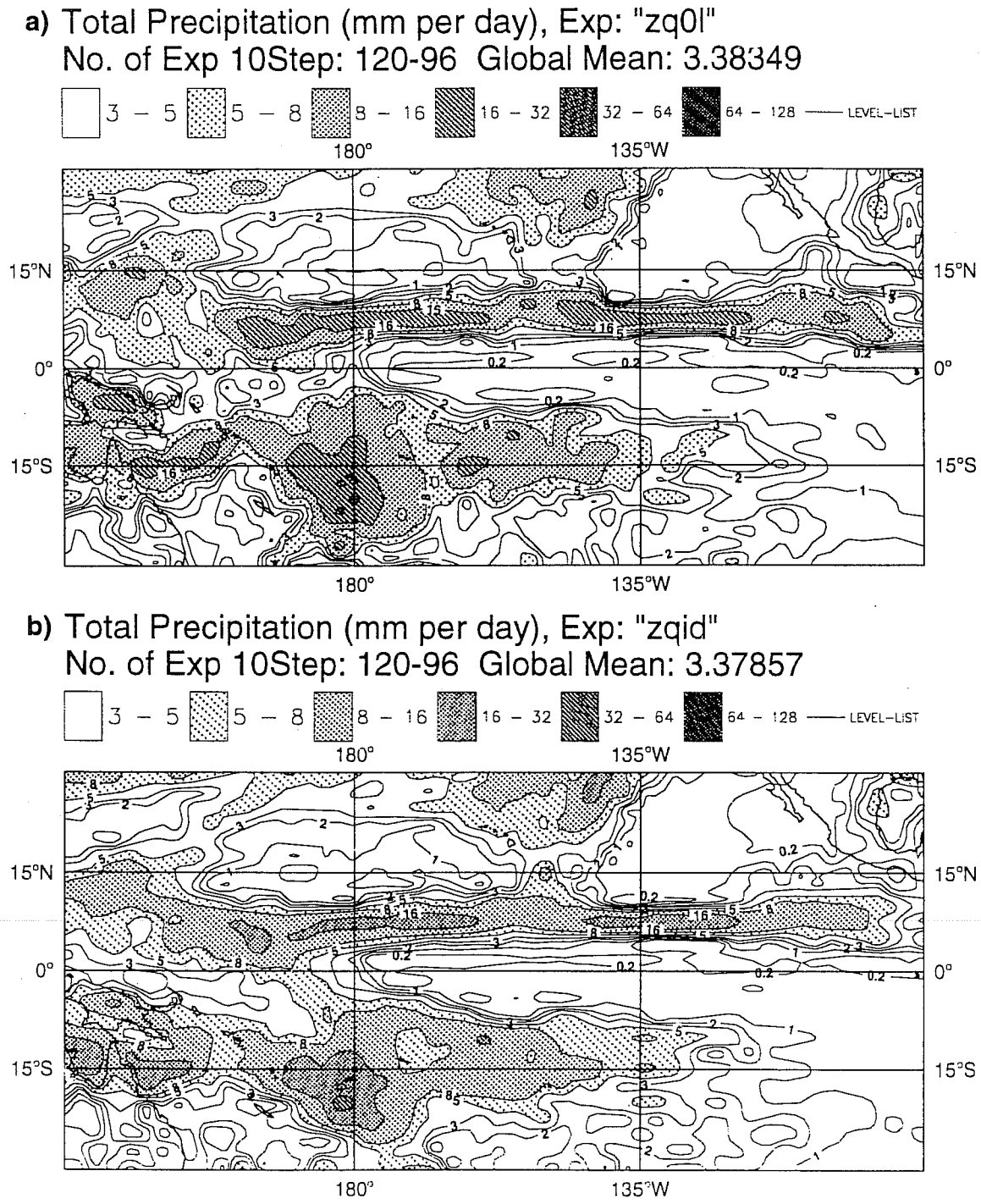

Fig. 24 Mean (16 cases) day 10 total precipitation (mm/day) over the Pacific from 4D-Var experimentation for January 1997. (a) Control forecasts; (b) PACKAGE F forecasts.